Let us assume a region of random irregular electron density structure located from $z = 0$ to $z = L$. A time-harmonic electromagnetic wave is incident on the irregular slab at $z = 0$ and received on the ground at $(\vec{r}, z)$. Let us consider that wave diffraction is due to a phase-changing irregular screen. As the wave passes through the irregularity slab, the ionosphere acts as a phase-changing screen that modifies only the phase of the wave. Therefore, upon emerging from the ionosphere, the wave measured by an interferometer element has the form (using Yeh and Liu, 1982, eq. (3.15)).

$$U(\vec{r}, \nu, z) = S_\nu \exp[\Psi(\vec{r}, \nu, z)] =$$

$$= S_\nu \exp[\chi(\vec{r}, \nu, z) - j\sigma_1(\vec{r}, \nu, z)]. \quad (6.2)$$

Without scintillation the ideal output of an interferometer with elements I and J can be written as

$$R_0(\nu, \vec{r}) = < S_{\nu I} \cdot S^*_{\nu J} > =$$

$$= S_\nu \int \exp\left[j 2\pi \frac{\nu_0}{c} \vec{B} \cdot \vec{r}_0\right] \int\int F(\nu) G(\vec{r} - \vec{r}_0) \cdot$$

$$\cdot \exp\left[j 2\pi \frac{\nu}{c} \vec{B} \cdot (\vec{r} - \vec{r}_0)\right] d\vec{r}\, d\nu\, dt \quad (6.3)$$

where S^* is the complex conjugate of S. When scintillation is present and the near field effects are also taken into account, the real output of an interferometer is

$$R(\nu, \vec{r}) = < U_{0I}(\vec{r}_I, \nu, z) \cdot U^*_{0J}(\vec{r}_J, \nu, z) > =$$

$$= < S_{\nu I} \cdot S^*_{\nu I} > \exp(\gamma\chi(\vec{r}_I, \nu, z) + \gamma\chi(\vec{r}_J, \nu, z)) \cdot$$

$$\cdot \exp(-j[\sigma_1(\vec{r}_I, \nu, z) - \sigma_1(\vec{r}_J, \nu, z)]) =$$

$$= R_0(\nu, \vec{r}) \exp(\gamma[\chi(\vec{r}_I, \nu, z) + \chi(\vec{r}_J, \nu, z)]) \cdot$$

$$\cdot \exp(-j[\sigma_1(\vec{r}_I, \nu, z) - \sigma_1(\vec{r}_J, \nu, z)]) \quad (6.4)$$

where the factor γ for the near field corrections can be written as (Spoelstra and Yang, 1995):

$$\gamma = \frac{2}{\pi \zeta \mu^2}\left[(\zeta \tan \beta_I)^2 \arccos\left(\frac{B}{\zeta\mu}\right) + \right.$$

$$\left. - \frac{1}{2}\left(\frac{B \tan \beta_I}{\mu}\right)^2 \tan\left\{\arccos\left(\frac{B}{\zeta\mu}\right)\right\}\right] +$$

$$+ \frac{2}{\pi \zeta \mu^2}\left[(\zeta \tan \beta_J)^2 \arccos\left(\frac{B}{\zeta\mu}\right) + \right.$$

$$\left. - \frac{1}{2}\left(\frac{B \tan \beta_J}{\mu}\right)^2 \tan\left\{\arccos\left(\frac{B}{\zeta\mu}\right)\right\}\right] \quad (6.5)$$

where ζ is the distance from the antenna towards the region of random irregular electron distribution, β_I is half the half-power-beamwidth of interferometer element I, β_J is half the half-power-beamwidth of interferometer element J and $\mu = (\tan \beta_I + \tan \beta_J)$. In relation (6.4) the term

$$\exp(\gamma[\chi(\vec{r}_I, \nu, z) + \chi(\vec{r}_J, \nu, z)]) \quad (6.4a)$$

refers to the log-amplitude of the wave or the amplitude scintillation, while the term

$$\exp(-j[\sigma_1(\vec{r}_I, \nu, z) - \sigma_1(\vec{r}_J, \nu, z)]) \quad (6.4b)$$

refers to the phase departure of the wave or the phase scintillation.

The complex correlator output of an interferometer is separated into a «real output» and an «imaginary output», which are also called «cos output» and «sin output», respectively. Then the amplitude and phase data are obtained as follows:

$$\text{amplitude data} = ([\text{cos output}]^2 + [\text{sin output}]^2)^{0.5} \quad (6.6)$$

and

$$\text{phase data} = \arctan\left[\frac{\text{sin output}}{\text{cos output}}\right]. \quad (6.7)$$

Correlated output is produced for all coherent contributions which enter both beams simultaneously. Near field contributions affect the measurements only if they appear in the overlapping parts of the both beams. This implies that both the cos and the sin components of these contributions should be multiplied with the factor γ since they are equally affected. From relations (6.6) and (6.7) it is clear that the amplitude component should be multiplied by this factor γ (as is done in relation (6.4)). The interferometer phase suffers from the usual different integrated refraction effects within the beams of each of the individual interferometer elements since the near field distortion cancels as is seen from relation (6.7). We note that this cancellation of the factor γ occurs at $B < (\xi\ (\tan\beta_I + \tan\beta_J))$. For $B \geqq (\xi\ (\tan\beta_I + \tan\beta_J))$ the resulting phase errors are the difference between the phase errors of the individual interferometer elements. Refraction effects cause phase errors which are to first order linearly proportional to the distance between the interferometer elements as long as the ionosphere is coherent over the interferometer baseline (Spoelstra, 1992a). This implies that the resulting scintillation in interferometer phase is the difference between the phase scintillation effects for each of the individual interferometer elements as we see from expression (6.4b) and linearly proportional to interferometer baseline.

6.2. *Amplitude scintillation*

When multiple scattering effects are not important, ionospheric irregularities of sizes of the first Fresnel zone are most effective in causing amplitude scintillation. The power spectrum of the fluctuations in ionospheric electron density is found to follow a power law (Dyson *et al.*, 1974; Sagalyn *et al.*, 1973). $\Phi_{\Delta N}(\kappa_p, \kappa_z)$ is the three dimensional spectrum of these density fluctuations. Here the z direction is along the line of sight. κ_p is the wavenumber of the fluctuations perpendicular to the line of sight.

For weak scintillation with $e^x \approx (1+x)$ [*i.e.* for $x \ll 1$] we can after some manipulation write for the field on the ground (Wernik and Liu, 1975; Yeh and Liu, 1982; Spoelstra and Yang, 1995)

$$S_4^2 \cong 4\pi^2 L \lambda^2 r_{el}^2 \int_{-\infty}^{+\infty} \int_{-\infty}^{+\infty} I(\vec{B}, \vec{\kappa}, \nu) \cdot$$

$$\cdot H(\vec{\kappa}, \nu, z) \Phi_{\Delta N}(\vec{\kappa}_p, 0) d^2\kappa_p \qquad (6.8)$$

where

$$H(\vec{\kappa}, \nu, z) =$$

$$= \left[1 - \frac{2k}{\kappa_p^2 L} \sin\left(\frac{\kappa_p^2 L}{2k}\right) \cos\left(\frac{\kappa_p^2}{k}\left(z - \frac{L}{2}\right)\right)\right], \qquad (6.9)$$

L is the thickness of the region of random irregular electron density structure, λ is the observing wavelength, r_{el} is the classical electron radius and k the wavenumber of the radio signal. The interferometer filter function $I(\vec{B}, \vec{\kappa}, \nu)$ can be written as

$$I(\vec{B}, \vec{\kappa}, \nu) = \gamma^2 [1 + \cos \vec{\kappa}_p \cdot \vec{B}]. \qquad (6.10)$$

This spatial interferometer filter function $I(\vec{B}, \vec{\kappa}, \nu)$ expresses the dependence of the scintillation index S_4 on interferometer baseline. This dependence is not present in the techniques which are commonly used to study ionospheric scintillation since in these techniques multiple antenna systems are not used in the interferometer mode as described here. Often radio interferometer systems consist of several tens of interferometer pairs at a variety of interferometer baselines. In addition to the fact that the scintillation index depends on the thickness of the slab $\sqrt{L}$, we note that since the factor γ is a function of interferometer baseline and of the altitude of the irregularities causing the scintillation, this height can be determined from the baseline dependence of the scintillation, index. Furthermore, we observe that the function $I(\vec{B}, \vec{\kappa}, \nu)$ is a function of the horizontal scale size (correlated with interferometer baseline), κ_p, which is characteristic for the irregularities causing the amplitude scintillation

in the observation considered. This implies that taking the observed baseline dependence of the scintillation index, the horizontal scale size of the irregularities can also be determined. Relation (6.10) is particularly sensitive for small scale irregularities, *i.e.* with linear scales of the same order as the interferometer baselines used and of the linear dimensions of the beam of the individual interferometer elements at the height at which the irregularities occur. Thus relation (6.8) indicates that from the observed baseline dependence of S_4 the altitude of the irregularities causing scintillation and their horizontal scale sizes can in principle be estimated. We note that this possibility is inherent to radio interferometry.

6.3. *Phase scintillation*

Similarly, we can derive after applying the Rytov solution according to Yeh and Liu (1982, see their relation (3.30)) and weighting the contribution to the phase scintillation by a spatial filter function $P(\vec{\kappa}, \nu, z)$ the manifestation of the diffraction effects inside the slab for the field on the ground (Spoelstra and Yang, 1995):

$$<S_1^2> = 4\pi^2 L \lambda^2 r_{el}^2 \int_{-\infty}^{+\infty} \int_{-\infty}^{+\infty} [1 - \cos \vec{\kappa}_p \cdot \vec{B}] \cdot$$

$$\cdot P(\vec{\kappa}, \nu, z)\, \Phi_{\Delta N}(\vec{\kappa}_p, 0)\, d^2 \kappa_p \qquad (6.11)$$

where

$$P(\vec{\kappa}, \nu, z) =$$

$$= \left[1 + \frac{2k}{\kappa_p^2 L} \sin\left(\frac{\kappa_p^2 L}{2k}\right) \cos\left(\frac{\kappa_p^2}{k}\left(z - \frac{L}{2}\right)\right)\right]. \qquad (6.12)$$

Or we can abbreviate relation (6.11) in a similar way as relation (6.8) as

$$<S_1^2> = 4\pi^2 L \lambda^2 r_{el}^2 \int_{-\infty}^{+\infty} \int_{-\infty}^{+\infty} Q(\vec{B}, \vec{\kappa}) \cdot$$

$$\cdot P(\vec{\kappa}, \nu, z)\, \Phi_{\Delta N}(\vec{\kappa}_p, 0)\, d^2 \kappa_p \qquad (6.13)$$

where

$$Q(\vec{B}, \vec{\kappa}) = [1 - \cos \vec{\kappa}_p \cdot \vec{B}] \qquad (6.14)$$

which includes the baseline dependence of phase scintillation effects in the interferometric observations.

The phase filtering function $P(\vec{\kappa}, \nu, z)$ and the interferometer filter function $Q(\vec{B}, \vec{\kappa})$ are very different from the corresponding functions for amplitude scintillation. It is easy to show from eq. (6.17) that $<S_1^2>$ increases with increasing interferometer baseline and that it decreases with ν^{-2}. The former relationship is well-known for phase errors due to refraction effects in radio interferometry (*e.g.*, Spoelstra, 1992a).

With the aid of the function $Q(\vec{B}, \vec{\kappa})$ it is in principle possible to estimate the characteristic horizontal linear scale sizes of the irregularities causing the phase fluctuations. Although this might seem straightforward, we should consider the fact that the interferometer phase errors due to ionospheric refraction effects are a complicated function of the geometry of the ionosphere and the electron distribution in this medium (Spoelstra, 1983). The scale sizes of the fluctuations causing scintillation as determined with the aid of function $Q(\vec{B}, \vec{\kappa})$ may be larger than the dimensions of the irregularities causing amplitude scintillation (*e.g.*, Yeh and Liu, 1982).

6.4. *Comparison with observations*

The formalism summarized in the previous sections was initially compared with observational data obtained with the east-west interferometer arrays WSRT and the Mi-yun Synthesis Radio Telescope, MSRT. The MSRT (40.56°N, 116.76°E). The maximum distances between two interferometer elements of the Mi-yun telescope is 1.15 km. The usual integration time is 10-30 s (Wang *et al.*, 1986). The MSRT operates at 232 and 327 MHz. The primary bean, of an element in the MSRT array is 10° at 232 MHz and 7° at 327 MHz. The primary

beam of an element in the WSRT array is 1.38° at 608.5 MHz and 2.6° at 327 MHz. The usual integration time is 10 s to 1 min.

For both the WSRT and MSRT observational examples have been selected (arbitrarily) for comparison with the approach discussed above.

An event on March 2, 1982, was selected for a more detailed investigation of scintillation effects in WSRT radio interferometric observations. An observation of 3C286 (right ascension α [1950.0] = 13 h 31 min 08.3 s, declination δ [1950.0] = +30°31′32.9″) was observed at 608.5 MHz during which significant scintillation occurred.

For observations with the MSRT the radio source Cyg A (right ascension α [1950] = 19 h 57 min 45 s, declination δ [1950] = +40°36′) is used for calibration purposes. Occasionally observations of Cyg A with the MSRT suffer from significant scintillation. We used for our analysis an observation made on September 20, 1985 (amplitude scintillation) and on August 26, 1986 (phase scintillation).

6.4.1. Amplitude scintillation

Amplitude scintillations were a common feature in the single dish observations made at 608.5 and 327 MHz, but they have never been observed in WSRT interferometer observations at baselines longer than 1 km. In general amplitude scintillation was only very seldom observed with the WSRT. Furthermore, this kind of scintillation was mainly observed during the night, while during the daytime it could not be distinguished from the instrumental noise.

For a power law spectrum $\Phi_{\Delta N} \propto \kappa_p^{-\eta}$, with an outer scale much greater than the Fresnel zone size, it is possible to show that

$$S_4 \propto \nu^{-(2+\eta)/4}. \qquad (6.15)$$

Simultaneous observations at 327 and at 608.5 MHz showed that $\eta = 3.5$ (± 0.6) (Spoelstra, 1985). This value agrees with the value of 4.0 ± 1.0 found by Rufenach (1972). Yeh and Liu (1980, 1982) found that the value of η shows some dependence on observing frequency.

A single dish radio telescope can be understood as an adding interferometer with zero baseline. Small changes within the beam of the instrument in the direction of the signal due to refraction may already cause diffraction patterns which cause the amplitude scintillation. In the case of amplitude scintillation the scintillation index includes spatial information about these irregularities and might suffer less from time-averaging if the integration time is shorter. Therefore, to study amplitude scintillation one might aim at integration times as short as possible.

For an instrument in which the interferometer elements are placed on an accurate east-west baseline as in the case of the MSRT and WSRT, relation (6.10) can be rewritten in a convenient form as

$$I(\vec{B}, \vec{\kappa}, \nu) = \gamma^2[1 + \cos(\kappa_p B \operatorname{cosec} \psi \sin \tau \cos \delta)] \qquad (6.16)$$

where ψ is the angle between the long axis of the irregularities (we assume that they are not spherical) causing scintillation and the local meridian, τ is the hour angle and δ the declination of the observed celestial radio source.

Figure 10a,b gives the relation of S_4^2 with B at about 2 h UT for the WSRT observation of March 2, 1982, as mentioned above. The elevation angle was about 67°. Figure 10a,b shows clearly that S_4^2 decreases with increasing B. When we take into account that the factor γ depends on height, the baseline dependence of the scintillation index depends on the altitude of the irregularities causing this scintillation. In order to check the validity of our approach in the previous sections we plotted in fig. 10a,b the function $I(\vec{B}, \vec{\kappa}, \nu)$ which gave the best fit on the data. In this case ν = 608.5 MHz, ζ = 150 km and κ_p cosec ψ = 0.05 m^{-1}. This implies that for the time of the observation the height of the region of random irregular electron distribution is the order 150 km. In addition we noted that the slab thickness of the F_2 layer determined from the analysis of the ionospheric Faraday rotation derived from the data of this observation is about 80 km (Spoelstra, 1985). In fig. 10a we also show calculations for ζ = 300 km and ζ = 75 km (indicated

by (2) and (3), respectively). In fig. 10b we show also results for κ_p cosec $\psi = 0.045$ m^{-1} and κ_p cosec $\psi = 0.055$ m^{-1} (indicated by (4) and (5), respectively).

If the irregularities are aligned along the geomagnetic field (*e.g.*, Kumagai, 1987), we take as the field declination (ψ in this case) for Westerbork a value of $-5°$. Then we estimated a horizontal size along the field as 230 m.

Figure 12a,b gives the relation of S_4^2 with B at about 1 h 30 UT for an observation of Cyg A with the MSRT at 232 MHz on September

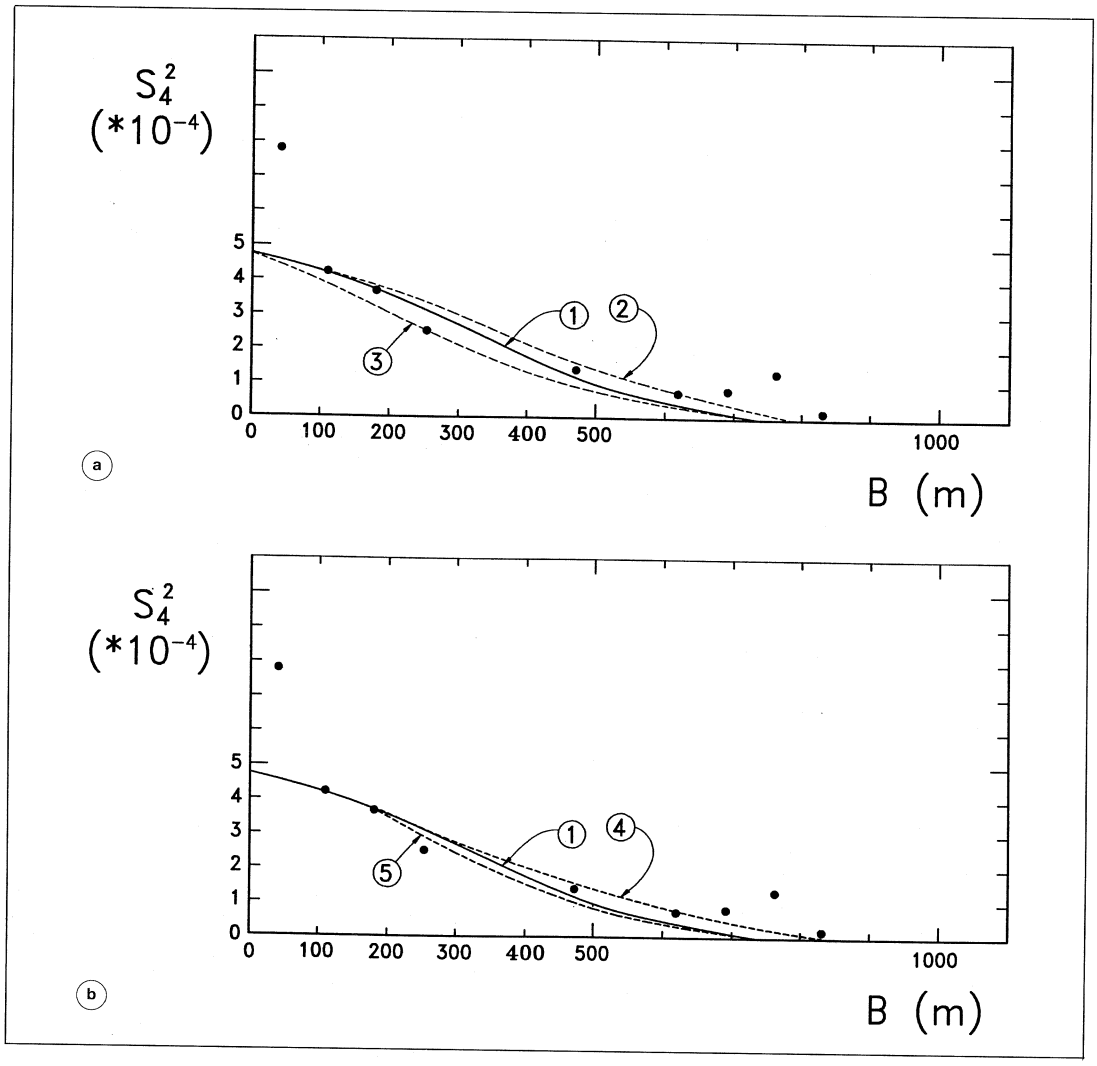

Fig. 10a,b. Scintillation index S_4^2 for an observation with the Westerbork Synthesis Radio Telescope on March 2, 1982, as a function of interferometer baseline B (meters). The curve shows the best fit of the filter function $I(\vec{B}, \vec{\kappa}, \nu)$ obtained for $\nu = 608.5$ MHz, $\zeta = 150$ km and κ_p cosec $\psi = 0.05$ m^{-1}. a) The figure shows also the calculations for $\zeta = 300$ km and $\zeta = 75$ km (indicated by (2) and (3), respectively); b) the solutions for κ_p cosec $\psi = 0.045$ m^{-1} and κ_p cosec $\psi = 0.055$ m^{-1} (indicated by (4) and (5), respectively).

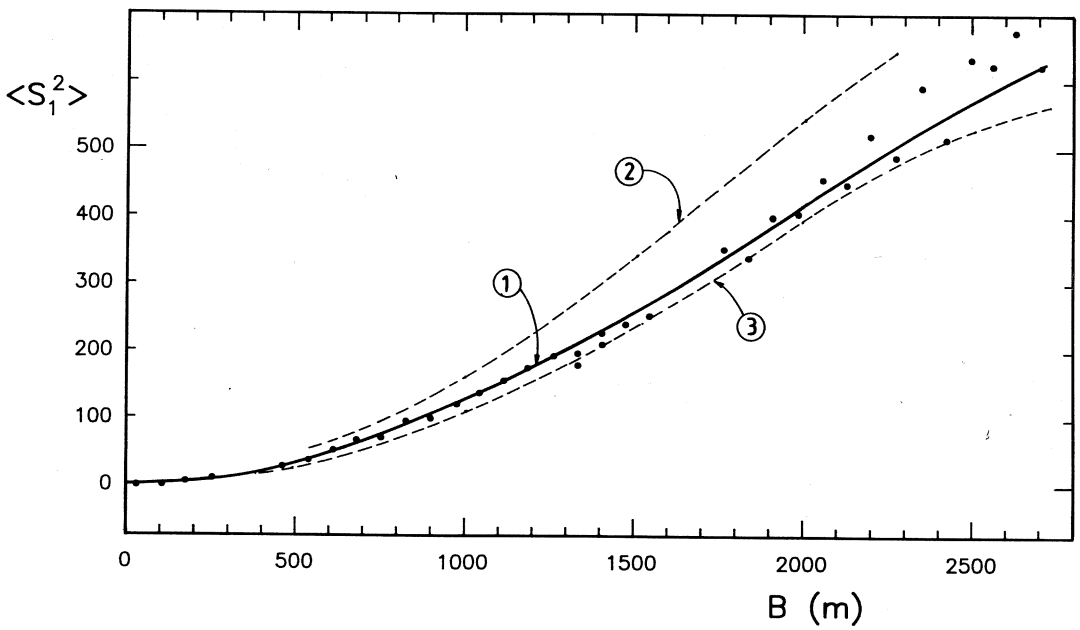

Fig. 11. Mean square phase fluctuations for the observation as used for fig. 10 a,b as a function of interferometer baseline B (meters). The curve shows the best fit of the function $Q(\vec{B}, \vec{\kappa})$ obtained for κ_p cosec $\psi = 0.01$ m^{-1}. The calculations for κ_p cosec $\psi = 0.011$ m^{-1} and κ_p cosec $\psi = 0.009$ m^{-1} are indicated by (2) and (3), respectively.

20, 1985. The elevation angle was about 65°. The baseline dependence of S_4^2 is clearly more complex than for the WSRT (fig. 10a,b). We also plotted in fig. 12a,b the function $I(\vec{B}, \vec{\kappa}, \nu)$ which gave the best fit on the data. In this case, $\nu = 232$ MHz, $\zeta = 150$ km and κ_p cosec $\psi = 0.015$ m^{-1}. This implies that for the time of the observation the height of the region of random irregular electron distribution is again of the order of 150 km. *If* the irregularities are aligned along the geomagnetic field (*e.g.*, Kumagai, 1987), we take as the field declination (ψ in this case) for Mi-yun a value of $-5.7°$. Then we estimate a horizontal size along the field as 650 m.

In fig. 12a,b we see that the filter curve fits well for baselines shorter than about 700 m. For longer baselines we expect an additional decrease of S_4^2 since at these baselines the radio source Cyg A can no longer be considered to be a point source. This effect is clearly seen since we derived the function $I(\vec{B}, \vec{\kappa}, \nu)$ only for point sources, *i.e.* source structure is not taken into account in the calculations of the curve in fig. 12a,b. In fig. 12a we also show calculations for $\zeta = 300$ km and $\zeta = 75$ km (indicated by (2) and (3), respectively). In fig. 12b we show also results for κ_p cosec $\psi = 0.018$ m^{-1} and κ_p cosec $\psi = 0.013$ m^{-1} (indicated by (4) and (5), respectively). We conclude that in fig. 12a,b the best fit is obtained for curve (1).

These examples indicate that the baseline dependence of S_4^2 is not very sensitive for the height of the irregularities causing the scintillation. But the characteristic horizontal scale of these irregularities is a very critical parameter: this parameter can be determined with an accuracy better than 10%. We also note that the baseline location of the maxima and minima in $I(\vec{B}, \vec{\kappa}, \nu)$ depends strongly on κ_p cosec ψ while the ratio between the different maxima is sensitive for ζ.

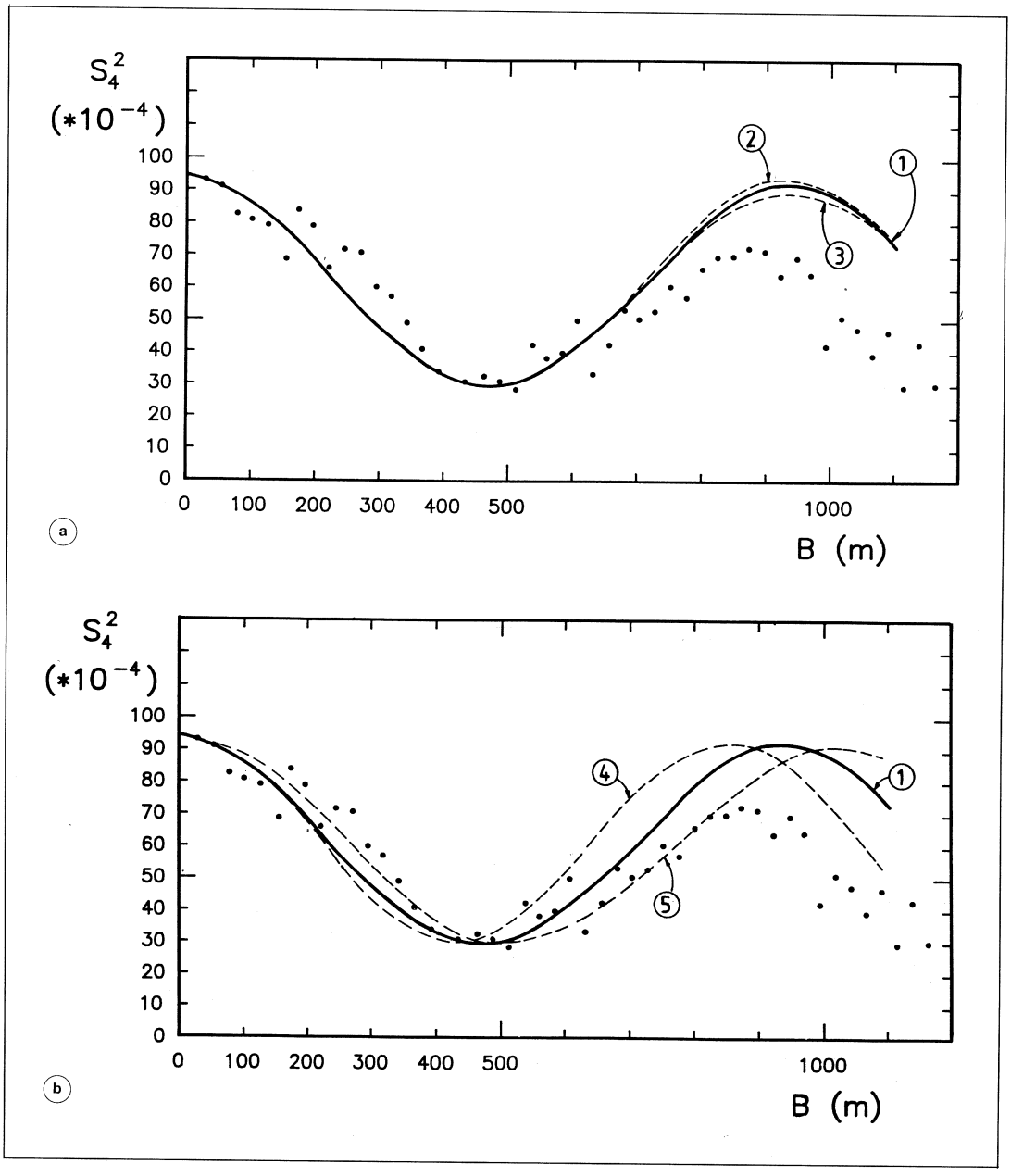

Fig. 12a,b. Scintillation index S_4^2 for an observation with the Mi-yun Synthesis Radio Telescope on September 20, 1985, as a function of interferometer baseline B (meters). The curve shows the best fit of the filter function $I(\vec{B}, \vec{\kappa}, \nu)$ obtained for $\nu = 232$ MHz, $\zeta = 150$ km and κ_p cosec $\psi = 0.015$ m^{-1}. a) The figure shows also the calculations for $\zeta = 300$ km and $\zeta = 75$ km (indicated by (2) and (3), respectively); b) the solutions for κ_p cosec $\psi = 0.018$ m^{-1} and κ_p cosec $\psi = 0.013$ m^{-1} are indicated by (4) and (5), respectively.

6.4.2. Phase scintillation

Phase scintillations have only been observed in *interferometric* observations. During the observing sessions only few (about 1 per month) scintillation events were recorded. Phase scintillation was only observed during the night.

Phase scintillation caused by ionospheric refraction due to small scale irregularities giving rise to large path length differences, of the order of the observing wavelength or more, will distort the interferometer amplitudes by decorrelation within the receiver if these irregularities occur within the integration time.

Phase fluctuations of the order of π radians or more within the integration time of 1 min correspond typically to irregularities with variations of about 1-10% in electron density. These phase scintillations may also be caused by severe distortion of the structure of the ionosphere as is shown by Spoelstra (1985).

In the case of phase scintillation integration times shorter than about 1 min presently used may not be very relevant either to avoid or to study short time scale irregularities. During an interval of 1 min the line of sight covers about 875 m at an altitude of 200 km.

For an instrument in which the interferometer elements are placed on an accurate east-west baseline as in the case of the WSRT and MSRT, relation (6.18) can be rewritten in a convenient form as

$$Q(\vec{B}, \vec{\kappa}) = [1 - \cos(\kappa_p B \operatorname{cosec} \psi \sin \tau \cos \delta)]. \tag{6.17}$$

We note that $Q(\vec{B}, \vec{\kappa})$ does not depend of course on ζ as function $I(\vec{B}, \vec{\kappa}, \nu)$ but only on κ_p and B.

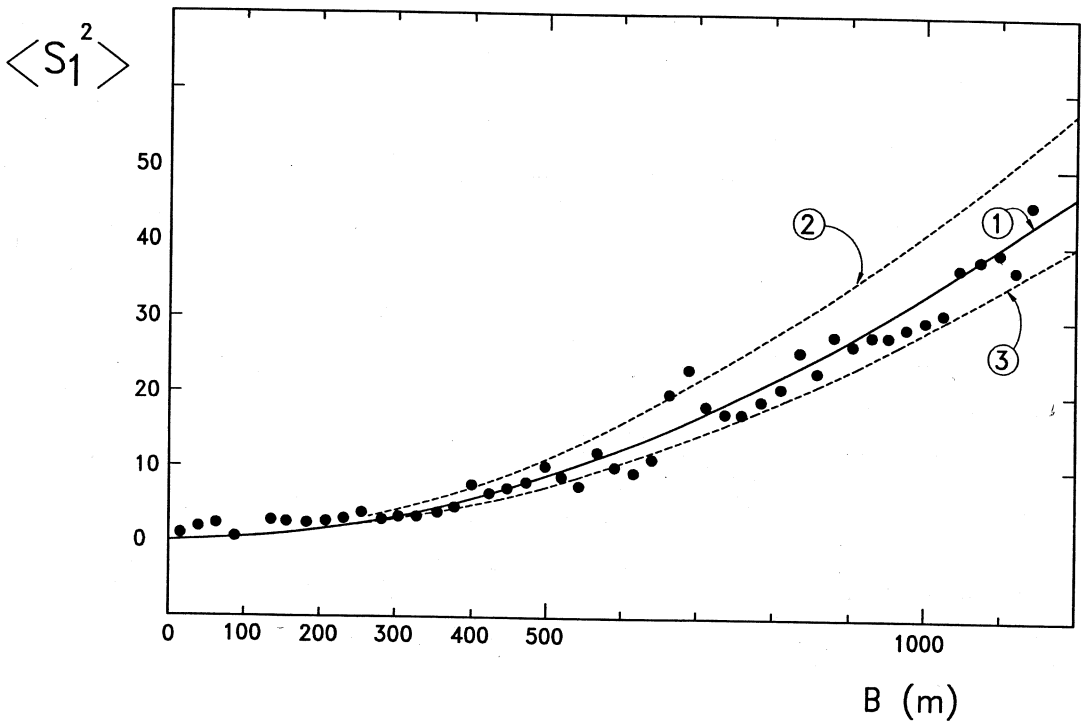

Fig. 13. Mean square phase fluctuations for an observation with the Mi-yun Synthesis Radio Telescope on August 26, 1986, as a function of interferometer baseline B (meters). The curve shows the best fit of the filter function $Q(\vec{B}, \vec{\kappa})$ obtained for κ_p cosec $\psi = 0.0067$ m^{-1}. The calculations for κ_p cosec $\psi = 0.0074$ m^{-1} and κ_p cosec $\psi = 0.0061$ m^{-1} are indicated by (2) and (3), respectively.

Figure 11 presents the mean square phase fluctuations at about 2 h UT for this observation as a function of baseline. It shows a gradual increase in phase fluctuations with baseline, which deviates from a linear relationship which we expect for «simple» refraction effects (Spoelstra, 1992a). In addition, we plotted the best fit of the function $Q(\vec{B}, \vec{\kappa})$. This fit holds for κ_p cosec $\psi = 0.01$ m^{-1}. In addition we plotted in fig. 11 the calculations for κ_p cosec $\psi = 0.011$ m^{-1} and κ_p cosec $\psi = 0.009$ m^{-1} (indicated by (2) and (3), respectively).

Figure 13 presents the mean square phase fluctuations at about 4 h 30 UT on August 26, 1986 for Cyg A as a function of baseline. The elevation angle was about 80°. Figure 13 shows a gradual increase of phase fluctuations with baseline, which deviates from a linear relationship which we expect for «simple» refraction effects (Spoelstra, 1992). In addition we plotted the best fit of the function $Q(\vec{B}, \vec{\kappa})$. This fit holds for κ_p cosec $\psi = 0.0067$ m^{-1}. In addition we plotted in fig. 13 the calculations for κ_p cosec $\psi = 0.0074$ m^{-1} and κ_p cosec $\psi = 0.0061$ m^{-1} (indicated by (2) and (3), respectively).

We note that the dimensions we derived from this analysis are typical for the scales of irregularities causing amplitude and phase scintillations (Booker, 1979). This analysis suggests also that the irregularities occurred in the lower areas of the F_2 layer.

From fitting the functions $I(\vec{B}, \vec{\kappa}, \nu)$ and $Q(\vec{B}, \vec{\kappa})$ to the data we estimate the accuracy with which the characteristic horizontal scale can be obtained conservatively as 10%. The altitude of the irregularities can be estimated with an accuracy of about 30%.

6.5. *Observing intense scintillation*

In the case of intense scintillation, multiple scattering effects become important. Let us assume a region of random irregular electron density structure located from $z = 0$ to $z = L$, *i.e.* its top-side and bottom-side, respectively. A time-harmonic electromagnetic wave is incident on the irregular slab at $z = 0$ and received on the ground at $(\vec{r}, z)$. In the case of strong scintillation the forward scattering assumption of the field at any height z' depends only on those irregularities in the region $z < z'$ and as the wave propagates in the random medium for a distance much greater than the longitudinal correlation distance of the fluctuating part characterizing the random variations caused by the irregularities of the dielectric permittivity $\varepsilon_1(\vec{r}, t)$, the field varies only a small amount in the correlation scale of $\varepsilon_1(\vec{r}, t)$, in the z direction.

Without scintillation the ideal output of an interferometer with elements I and J can be written as elation (6.3). Following Yeh and Liu (1982) we write for the coherence function

$$\Gamma_2(\vec{r}, \vec{r}', \nu, z) = \langle U(\vec{r}, \nu, z) \cdot U^*(\vec{r}', \nu, z) \rangle = \\ = R_0 \exp\left(-\frac{1}{2} D_{\Delta\phi}(\vec{r} - \vec{r}')\right) \qquad (6.18)$$

where U^* is the complex conjugate of U: the optical path structure function $D_{\Delta\phi}(\vec{r} - \vec{r}')$ is defined by Yeh and Liu (1982) as

$$D_{\Delta\phi}(\vec{r} - \vec{r}') = 2C^2 z[A_{\Delta N}(0) - A_{\Delta N}(\vec{r} - \vec{r}')] \qquad (6.19)$$

where $C = e^2/(2m\varepsilon_0\omega^2)$, e is the electronic charge, m is its mass, ε_0 is the free space permittivity, ω is the circular radio frequency and

$$A_{\Delta N}(\vec{r}) = 2\pi \int_{-\infty}^{+\infty} \int_{-\infty}^{+\infty} \Phi A_{\Delta N}(\vec{\kappa}_p, 0) \exp(j \vec{\kappa}_p \cdot \vec{r})\, d^2\kappa_p \qquad (6.20)$$

in which $\Phi_{\Delta N}(\kappa_p, \kappa_z)$ is the three dimensional spectrum of these density fluctuations. Here the z direction is along the line of sight. κ_p is the wavenumber of the fluctuations perpendicular to the line of sight.

The coherence function Γ_4 for two interferometer elements I and J can be written (following the commonly used definition) as

$$\Gamma_4(\vec{r}, \vec{r}', \nu, z) = \langle U(\vec{r}_I, \nu, z) \cdot \\ \cdot U(\vec{r}_J, \nu, z) \cdot U^*(\vec{r}'_I, \nu, z) \cdot U^*(\vec{r}'_J, \nu, z) \rangle. \qquad (6.21)$$

Then

$$\frac{\partial \Gamma_4}{\partial z} = -\frac{j}{2k}[\nabla_I^2 + \nabla_J^2 - \nabla'^2_I - \nabla'^2_J]\,\Gamma_4 +$$

$$-\frac{1}{2L}[D_{\Delta\phi}(\vec{r}_I - \vec{r}\,'_I) + D_{\Delta\phi}(\vec{r}_I - \vec{r}\,'_J) +$$

$$+D_{\Delta\phi}(\vec{r}_J - \vec{r}\,'_I) + D_{\Delta\phi}(\vec{r}_J - \vec{r}\,'_J) +$$

$$-D_{\Delta\phi}(\vec{r}_I - \vec{r}\,'_J) - D_{\Delta\phi}(\vec{r}\,'_I - \vec{r}\,'_J)]\,\Gamma_4 \quad (6.22)$$

where $\nabla_i^2 = \frac{\partial^2}{\partial x_i} + \frac{\partial^2}{\partial y'_i}$, $\nabla'^2_i = \frac{\partial^2}{\partial x'_i} + \frac{\partial^2}{\partial y'_i}$ and $D_{\Delta\phi}(\vec{r})$ is the structure function for the phase fluctuations defined in eq. (6.18). Assuming that the interferometer baseline $\vec{B} = (\vec{r}_I - \vec{r}_J)$ and $\vec{\Xi}_{IJ} = (\vec{r}_I - \vec{r}\,'_J)$ we may rewrite relation (6.21) as

$$\frac{\partial \Gamma_4}{\partial z} = -\frac{j}{2k}[\nabla_I^2 + \nabla_J^2 - \nabla'^2_I - \nabla'^2_J]\,\Gamma_4 +$$

$$-\frac{1}{2L}[D_{\Delta\phi}(\vec{\Xi}_{II}) + D_{\Delta\phi}(\vec{B} + \vec{\Xi}_{JJ}) +$$

$$+D_{\Delta\phi}(-\vec{B} + \vec{\Xi}_{II}) + D_{\Delta\phi}(\vec{\Xi}_{JJ}) +$$

$$-D_{\Delta\phi}(\vec{B}) - D_{\Delta\phi}(\vec{B} - \vec{\Xi}_{II} + \vec{\Xi}_{JJ})]\,\Gamma_4. \quad (6.23)$$

In radio interferometry the correlation of signals from the same source can be done if the signals are collected by coincident parts of the antenna patterns of the different interferometer elements. When scintillation is present and the near field effects are also taken into account, we assume random variations caused by the isotropic irregularities we may take $\vec{\Xi}_{II} = \vec{\Xi}_{JJ} = \vec{\Xi}$, so that relation (6.22) becomes

$$\frac{\partial \Gamma_4}{\partial z} = -\frac{j\,\Upsilon(\gamma)}{2k}[\nabla_1^2 + \nabla_2^2 - \nabla'^2_1 - \nabla'^2_2]\,\Gamma_4 +$$

$$-\frac{\Upsilon(\gamma)}{2L}[2D_{\Delta\phi}(\vec{\Xi}) + D_{\Delta\phi}(\vec{B} + \vec{\Xi}) +$$

$$+D_{\Delta\phi}(-\vec{B} + \vec{\Xi}) - 2D_{\Delta\phi}(\vec{B})]\,\Gamma_4 \quad (6.24)$$

where $\Upsilon(\gamma)$ is a function of the factor γ for the near field corrections. We emphasize that the approximation in relation (6.24) is valid since correlated output is produced for all coherent contributions which enter both beams simultaneously. Near field contributions affect the measurements only if they appear in the overlapping parts of the both beams. We note that $\gamma = 1$ for $B = 0$ and $\gamma = 0$ if $B \geqq \zeta\mu$ (since physically it cannot become negative). Because γ is a function of altitude (since the horizontal cross section of the antenna beam depends on altitude) we introduce a function $\Upsilon(\gamma)$ to take into account the correlated contributions along the line of sight.

For weak scintillation $\Upsilon(\gamma) = \gamma^2$, which corresponds with the thin phase screen approximation. In the case of intense scintillation

$$\Upsilon(\gamma) = \frac{1}{4}(\gamma_{\zeta=\zeta_{\max}} + \gamma_{\zeta=\zeta_{\max}-\zeta_z})^2 \quad (6.25)$$

as can easily be seen from Spoelstra and Yang (1995); here $\zeta_{\max}$ is the altitude of the topside of the irregular electron density structure and ζ_z the bottom location (depending on the baseline $\vec{B}$) within this structure while $0 \leqq z \leqq L$. We can write ζ_z as

$$\zeta_z = \zeta_{\max} - L$$

$$\text{for } 0 \leqq B \leqq (\zeta_{\max} - L)(\tan\beta_I + \tan\beta_J) \quad (6.26)$$

and

$$\zeta_z = \frac{B}{\tan\beta_I + \tan\beta_J} \quad (6.27)$$

for $(\zeta_{\max} - L)(\tan\beta_I + \tan\beta_J) \leqq B \leqq \zeta_{\max}(\tan\beta_I + \tan\beta_J)$, which implies that $\gamma_{\zeta=\zeta_{\max}-\zeta_z} = 0$ for these baselines.

Using the definition of eq. (6.19) we may rewrite formula (6.18) as

$$D_{\Delta\phi}(\vec{r} - \vec{r}\,') = 4\pi C^2 z\Big[\int_{-\infty}^{+\infty}\int_{-\infty}^{+\infty} \Phi_{\Delta N}(\vec{\kappa}_p, 0)\,d^2\kappa_p +$$

$$-\int_{-\infty}^{+\infty}\int_{-\infty}^{+\infty} \Phi_{\Delta N}(\vec{\kappa}_p, 0)\exp(j\,\vec{\kappa}_p \cdot [(\vec{r} - \vec{r}\,')])\,d^2\kappa_p \quad (6.28)$$

so that eq. (6.24) becomes

$$\frac{\partial \Gamma_4}{\partial z} = -\frac{j\,\Upsilon(\gamma)}{2k}\,[\nabla_I^2 + \nabla_J^2 - \nabla_I'^2 - \nabla_J'^2]\,\Gamma_4 +$$

$$-4\pi C^2 z\,\frac{\Upsilon(\gamma)}{2L}\,[2\{\int_{-\infty}^{+\infty}\int_{-\infty}^{+\infty} \Phi_{\Delta N}(\vec{\kappa}_p, 0)\, d^2\kappa_p +$$

$$-\int_{-\infty}^{+\infty}\int_{-\infty}^{+\infty} \Phi_{\Delta N}(\vec{\kappa}_p, 0) \exp(j\vec{\kappa}_p \cdot \vec{\Xi})\, d^2\kappa_p\} +$$

$$+\{\int_{-\infty}^{+\infty}\int_{-\infty}^{+\infty} \Phi_{\Delta N}(\vec{\kappa}_p, 0)\, d^2\kappa_p +$$

$$-\int_{-\infty}^{+\infty}\int_{-\infty}^{+\infty} \Phi_{\Delta N}(\vec{\kappa}_p, 0) \exp(j\vec{\kappa}_p \cdot [\vec{B} + \vec{\Xi}])\, d^2\kappa_p\} +$$

$$+\{\int_{-\infty}^{+\infty}\int_{-\infty}^{+\infty} \Phi_{\Delta N}(\vec{\kappa}_p, 0)\, d^2\kappa_p +$$

$$-\int_{-\infty}^{+\infty}\int_{-\infty}^{+\infty} \Phi_{\Delta N}(\vec{\kappa}_p, 0) \exp(j\vec{\kappa}_p \cdot [-\vec{B} + \vec{\Xi}])\, d^2\kappa_p\} +$$

$$-2\{\int_{-\infty}^{+\infty}\int_{-\infty}^{+\infty} \Phi_{\Delta N}(\vec{\kappa}_p, 0)\, d^2\kappa_p +$$

$$-\int_{-\infty}^{+\infty}\int_{-\infty}^{+\infty} \Phi_{\Delta N}(\vec{\kappa}_p, 0) \exp(j\vec{\kappa}_p \cdot \vec{B})\, d^2\kappa_p\}]\,\Gamma_4. \tag{6.29}$$

If we observe point sources, *i.e.* if the incident wave front is flat, $\nabla_i = 0$ and we can set $\vec{\Xi} = 0$ in (6.24) without loss of generality. Then eq. (6.29) becomes

$$\frac{\partial \Gamma_4}{\partial z} = -4\pi C^2 z\,\frac{\Upsilon(\gamma)}{2L}\cdot$$

$$\cdot[\int_{-\infty}^{+\infty}\int_{-\infty}^{+\infty} \Phi_{\Delta N}(\vec{\kappa}_p, 0)\, \exp(j\vec{\kappa}_p \cdot \vec{B})\, d^2\kappa_p +$$

$$-\int_{-\infty}^{+\infty}\int_{-\infty}^{+\infty} \Phi_{\Delta N}(\vec{\kappa}_p, 0) \exp(j\vec{\kappa}_p \cdot \vec{B})\, d^2\kappa_p]\,\Gamma_4 \tag{6.30}$$

which has the form

$$\frac{\partial \Gamma_4}{\partial z} = -\frac{\Upsilon(\gamma)}{2L}\,E(\vec{r}_I, \vec{r}_J)\,\Gamma_4. \tag{6.31}$$

For a power-law irregularity spectrum of the form

$$\Phi_{\Delta N}(\vec{\kappa}_p) = C_N^2 |\vec{\kappa}_p|^{-\eta} \tag{6.32}$$

we can write (analogously to Yeh and Liu, 1982):

$$\frac{\partial \Gamma_4}{\partial z} = -\Upsilon(\gamma)\Gamma_4 \int_{-\infty}^{+\infty}\int_{-\infty}^{+\infty} |\vec{\kappa}_p|^{-\eta}(1 - \cos \vec{\kappa}_p \cdot \vec{B})\, d^2\kappa_p \tag{6.33}$$

and with an initial condition $\Gamma_4 = R_0^2$ at $z = Z = 0$ (*i.e.*, for a wave incident at the top-side of the irregular electron density structure). For $z > L$ (*i.e.*, for a wave emerging from the bottom-side of the irregular electron density structure), eq. (6.33) becomes

$$\frac{\partial \Gamma_4}{\partial z} = 0, \qquad \text{for } z > L \tag{6.34}$$

with Γ_4 at $z = L$ as its «initial» condition, implying that Γ_4 is not a function of z for $z > L$. This means that the signal emerging from the bottom-side of the irregular electron density structure is the incident signal affected by the medium as expressed by Γ_4.

The solution of eq. (6.33) must be independent of the irregularity strength and the geometry since it is dimensionless. The relation between Γ_4 and the scintillation index S_4 can be expressed as

$$S_4^2 = \Upsilon(y)\left(\frac{1}{R_0^2}\,\Gamma_4(z, \vec{B}) - 1\right). \tag{6.35}$$

This expression shows that the scintillation index is a function of z and $\vec{B}$. The scintillation index S_4 is an observational parameter which can be determined as a function of interferometer baseline $\vec{B}$. The baseline dependence of S_4^2 is proportional to the function $\Upsilon(\gamma)$.

6.6. *Intense scintillation observations*

If the beams of the two interferometer elements are equal, eq. (6.5) simplifies to

$$\gamma = \frac{2}{\pi}\left[\arccos\left(\frac{B}{2\zeta\tan\beta}\right) + -\left(\frac{B}{2\zeta\tan\beta}\right)^2 \tan\left\{\arccos\left(\frac{B}{2\zeta\tan\beta}\right)\right\}\right] \quad (6.36)$$

where 2β is the half-power beamwidth of an interferometer element. The geometry for beam coverages of interferometer elements is given in fig. 14.

Observations of intense scintillation with the OSRT as a function of east-west baseline are presented in fig. 15a,b for a source at right ascension α (1950.0) = 11 h 17 min 40.0 s, declination δ (1950.0) = + 13°52′06.0″. This example is arbitrary and many more can be added.

From eq. (6.35) it is obvious that differences of the observed S_4^2 from the function $\Upsilon(\gamma)$ which are a function of baseline $\vec{B}$, depend on the interferometer response R_0 and on the function $\Gamma_4(z, \vec{B})$. If the observed radio source is a perfect point source R_0 is independent of interferometer baseline. Assuming that this case is valid for the examples studied, or taking a more realistic approach by assuming a very weak baseline dependence of R_0 deviations of S_4^2 from $\Upsilon(\gamma)$ reflect the function $\Gamma_4(z, \vec{B})$ which implies that we may experimentally estimate this function by using radio interferometry. Or we may state that in the case of *intense* scintillation the baseline dependence of S_4^2 and of $\Upsilon(\gamma)$ are the same, provided the influences of $\Gamma_4(z, \vec{B})$ are known. This similarity differs

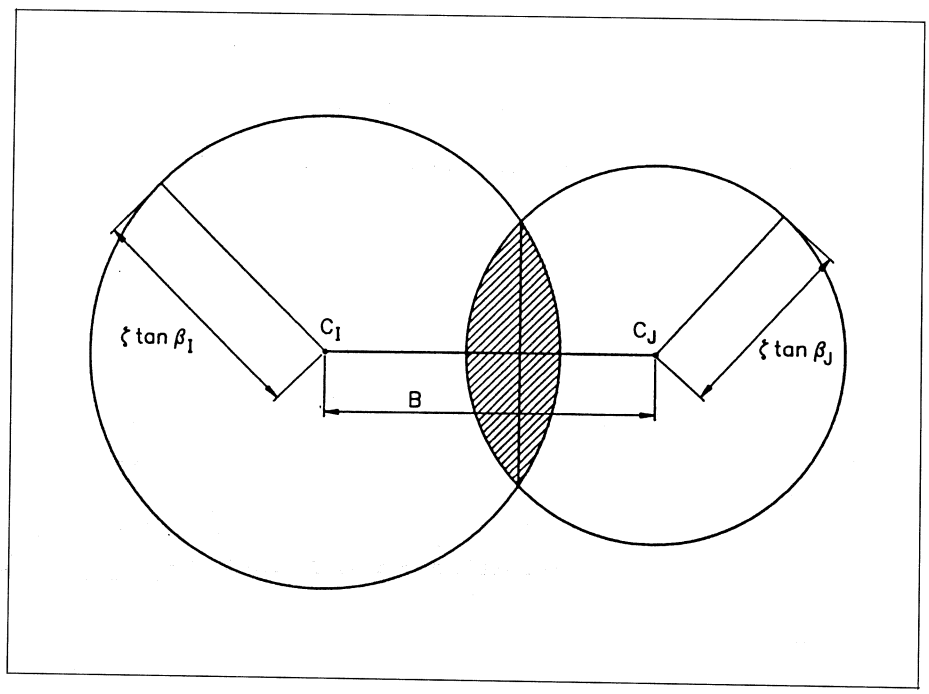

Fig. 14. Schematic diagram showing the coverages of the beams of interferometer elements with identical beams through the irregular electron density structure.

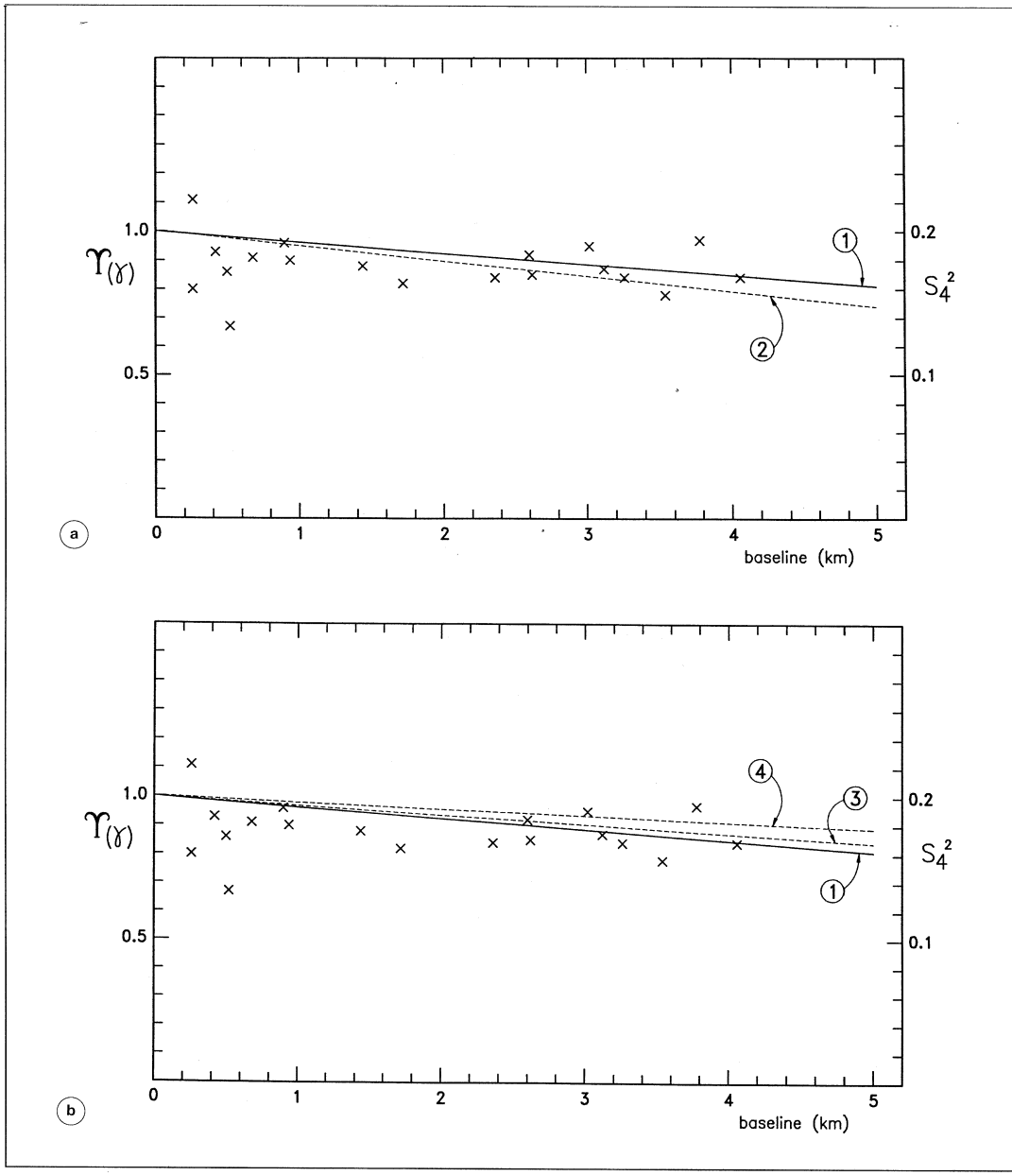

Fig. 15a,b. a) Observations of intense scintillation with the OSRT as a function of east-west baseline are presented for a source at right ascension α (1950.0) = 11 h 17 min 40.0 s, declination δ (1950.0) = +13°52′06.0″. Observing date: 27 October 1985. Observing time: 15 h 06 min UT. The function $\Upsilon(\gamma)$ for ζ_{max} = 850 km and L = 700 km is given by the curve (1). Curve (2) gives the calculations for ζ_{max} = 250 km and L = 100 km. b) as (a). Curve (3) gives the calculations for ζ_{max} = 600 km and L = 400 km and curve (4) for ζ_{max} = 800 km and L = 400 km.

from the case of weak scintillation (Spoelstra and Yang, 1995).

If the irregularities causing the scintillation are aligned along the geomagnetic field (*e.g.*, Kumagai, 1987), we rewrite eq. (6.33) as

$$\frac{\partial \Gamma_4}{\partial z} = -\Upsilon(\gamma)\Gamma_4 \int_{-\infty}^{+\infty}\int_{-\infty}^{+\infty} |\vec{\kappa}_p|^{-\eta} \cdot [1 - \cos(\kappa_p B \operatorname{cosec}\psi \sin\tau\cos\delta)]\, \mathrm{d}^2\kappa_p \quad (6.37)$$

where ψ is the angle between the long axis of the irregularities (we assume that they are not spherical) causing scintillation and the local meridian (*i.e.*, ψ is the geomagnetic declination). Given these dependences the deviations of S_4^2 from $\Upsilon(\gamma)$ manifest the dependence of Γ_4 on both z and $\vec{B}$. This is implied in the differences between *e.g.*, the OSRT data and the calculated $\Upsilon(\gamma)$ values. We may assume that for $B \leqq (\zeta_{\max} - L)(\tan\beta_I + \tan\beta_J)$ the value for Z in Γ_4 does not vary, so that then the dependence of Γ_4 on $\vec{B}$ may be estimated (if possible). For $(\zeta_{\max} - L)(\tan\beta_I + \tan\beta_J) \leqq B \leqq \zeta_{\max}(\tan\beta_I + \tan\beta_J)$ the dependence of Γ_4 on z and on $\vec{B}$ are coupled.

In fig. 15a,b the function $\Upsilon(\gamma)$ for $\zeta_{\max} = 850$ km and $L = 700$ km (*i.e.*, a very large part of the ionosphere is taken) is shown for baselines up to 5 km for the OSRT. We note that the baselines used were not large enough to give a full account of function $\Gamma_4(z, \vec{B})$, since we expect from eq. (6.35) that for $z = 0$ $S_4^2 = 0$, which has not been observed. This indicates that for $\zeta_{\max} = 850$ km $\Upsilon(\gamma) = 0$ for baselines $B \gtrsim 100$ km in the case of OSRT measurements. Since these baselines do not exist, it is understandable that OSRT observations will suffer severe scintillation (if present) at all baselines with S_4 almost independent of interferometer baseline. This estimate is, however, rather rough since it depends very much on the fit of $\Upsilon(\gamma)$ through the data, which is a function of $\zeta_{\max}$ and L as is shown in fig. 15a,b. Figure 15a,b illustrates that $\Upsilon(\gamma)$ is more sensitive for $\zeta_{\max} - L$) with fixed L, *i.e.*, the minimum value of $\zeta(= \zeta_{\min})$, than for a fixed value of $\zeta_{\min}$ while both $\zeta_{\max}$ and L vary. Thus $\zeta_{\min}$ mainly determines $\Upsilon(\gamma)$ for a given baseline and beamwidth.

The GMRT is a two dimensional array consisting of 30 telescopes each with a diameter of 45 m has baselines up to about 25 km. The geomagnetic latitude of this station is about 7.5°, *i.e.*, in the region of the equatorial anomaly. This means that the observations at this station will suffer severely from the equatorial ionosphere. Considering the ionospheric conditions during the OSRT observation given in fig. 15a,b the GMRT would need at a frequency of 327 MHz baselines of at least 15 km to achieve a condition of $\Upsilon(\gamma) = 0$. For the lower frequencies at which this instrument will operate the baseline at which $\Upsilon(\gamma) = 0$ would need to be proportionally longer.

6.7. *Concluding remarks on scintillation*

Radio interferometry turns out to provide a powerful tool to determine structural information in terms of space and time of small scale ionospheric irregularities causing amplitude and phase scintillation. In particular, the dependence of the measured scintillation index and the mean square phase fluctuations on interferometer baseline turns out to provide a key parameter. This is especially the case when these parameters are measured for a range of different interferometer baselines. We note, however, that our analysis of some data is still very simple and that the estimates for the horizontal scale sizes are highly dependent upon the angle and the degree of alignment between the irregularities and the geomagnetic field. Furthermore, the parameter ψ may also vary within the antenna beams. To imply this means that all integrations over κ_p have to be performed over ψ as well. In case a two dimensional interferometer is used, reasonable estimates for ψ can also be made. Furthermore, radio interferometry may provide a tool to determine the structure function $\Gamma_4(z, \vec{B})$ affecting the transionospheric radio signal to suffer from intense scintillation.

From this simple analysis in the present paper we conclude that the ionospheric irregularities causing scintillation may occur in the lower parts of the F_2-layer. The spatial scale of irregularities causing amplitude scintillation is

of the order of about 25 to about 500 m. Phase scintillations are caused by irregularities with dimensions which are an order of magnitude larger. These results are well in agreement with results obtained by other investigaters (*e.g.*, Booker, 1979).

Although the examples discussed above have been selected arbitrarily, we have taken them, on the basis of scintillation occurrence, of course. However, there are indications that during these events the geomagnetic field was significantly distorted (Cander and Jodogne, private communication).

A second result of this analysis is that intense scintillation, which is a common phenomenon at low geomagnetic latitudes, cannot be avoided by using long baselines, unless very long baselines are used. If the baselines become of the scale of those used in VLBI it reenters the data again as scintillation effects in signals from the individual interferometer elements.

7. Quiet/disturbed conditions in the ionosphere

In the evaluation of the results of the analysis of the climatology of ionospheric irregularities (sections 5 and 6), an important question is the definition of a «disturbed» condition of the medium. Initially one may say that «disturbed» means «everything deviating from the expectations». These expectations, however, have to be based on *a priori* experimental knowledge. Implicitely they depend on some instrument used, usually in particular an ionosonde. The fact that the antenna beam of an ionosonde is typically about 45° or more implies that this instrument is not sensitive for effects of ionospheric irregularities of smaller angular scale. The *a priori* experimental knowledge depends of course heavily on the application. Extrapolating from the usual ionosonde data, we define «quiet» as the *monthly median values of parameters derived from ionosonde measurements* since these imply a smooth condition. Then «disturbed» may be defined as *deviations from these monthly median values.* One may object that the period of a month is too long: this has been taken to enable the detection of disturbances with a duration of the order of days, *e.g.*, manifestations of magnetic storms.

The next problem involves a quantity which indicates a «Disturbance Measure», DM, to express how severe the disturbance is. It is clear that the effect of the DM on the experimental data depends on the frequency and technique used. The frequency dependence of DM is related to the frequency dependence of the refractive index. The dependence of DM on the technique used is related to the extent that specific propagation effects can be detected with the application used.

If we use the definition for «quiet», which is of course also dependent on the geographic location of the used instrument, we may define the «disturbance measure» as the *magnitude of the variations of the gradients in the ionospheric electron density distribution.* This is justified since disturbance as a concept means always «something» superimposed on «some parameter». In propagation matters the magnitude of the variations are of most concern in discussions about the «quietness» of the medium. On the other hand, when using the expression «variations of the gradients in the ionospheric electron distribution» we account for the quantitative deviations from the reference parameter, *i.e.*, the monthly median values of parameters derived from ionosonde measurements. Thirdly, a dependence on time, *e.g.*, to cope with day or night values, should not be included explicitly in the definition itself since the parameters referred to in the definition are a function of time by nature. Since the reference for DM consists of the monthly median values of ionosonde data, DM refers to deviations from these in terms of *vertical* electron content quantities.

As an example (in particular applicable to connected element interferometry), the Disturbance Measure, DM, at some specific moment is the amplitude of the variation in gradients in TEC derived from interferometer phase measurements.

Connected radio interferometers such as the WSRT are primarily sensitive to horizontal and

vertical *gradients* in the ionospheric electron distribution (Spoelstra, 1983). The 0th order effects which are related to parameters derived from ionosonde measurements cannot be derived from the interferometer data directly. Therefore, the variations in interferometer phase translated in terms of variations in ionospheric electron density are manifestations of the disturbances on the quiet ionosphere. As a function of time the amplitude of these variations indicates directly how severe the disturbances in the ionosphere are. The frequency of occurrence as a function of time indicates the probability that the disturbed condition of the ionosphere is to be expected. Estimates of the frequency of occurrence are directly associated with the amplitude of the variations, since one may want to know the frequency of occurrence of variations above some specified threshold or above some specific DM.

7.1. *Quiet and disturbed periods*

Figures 16 and 17 show the fraction of time that the ionosphere is disturbed with a noise above a certain disturbance measure threshold. For fig. 16 this threshold is $10^{11}\mathrm{m}^{-3}$, for fig. 17 it is $2\times10^{11}\mathrm{m}^{-3}$. This fraction of time is given as a function of time in the day per season as a function of year. For the frequency of occurrence of TIDs the reader is referred to section 5.1. The enhancements in a number of seasons and years (*e.g.*, the Summer periods in the early 70s) may suffer from tropospheric effects in 21 cm observations as discussed in the previous section.

We observe that noise in interferometer phase larger than 10° interferometer phase at 49 cm wavelength and a baseline of 1.5 km (corresponding with about $7\times10^{10}\mathrm{m}^{-3}$) is a common phenomenon. The instrumental noise in interferometer phase is about 0.5° at this baseline corresponding with about $0.4\times10^{10}\mathrm{m}^{-3}$. For a DM level of $2\times10^{11}\mathrm{m}^{-3}$ the fraction of time that the ionosphere is disturbed with noise shows a pattern very similar to the results of the frequency of occurrence of TIDs (Spoelstra, 1996). This implies a common origin for both phenomena.

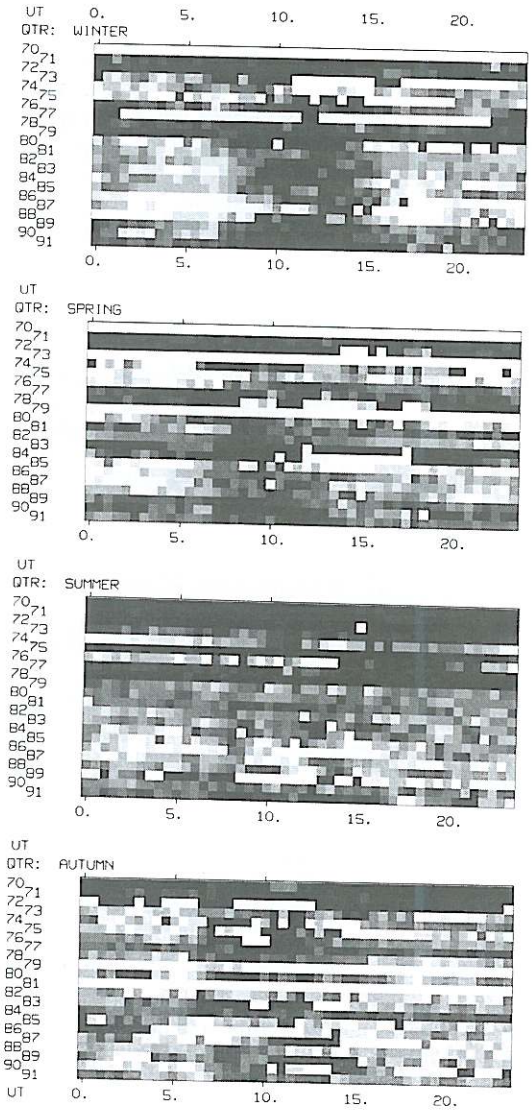

Fig. 16. Fraction of time that the ionosphere is disturbed above a certain disturbance measure, DM. In this figure this level is $10^{11}\mathrm{m}^{-3}$. This fraction is given as a function of time in the day per season as a function of year. The horizontal axis indicates the time in UT hours. The ordinate indicate the year. The fraction is represented in %: the values are expressed by grey scale levels. The grey levels intervals are: 20-30, 30-40, 40-50, 50-60, 60-70, 70-80, 80-90 and > 90 %. White indicates that there are not enough data for that bin.

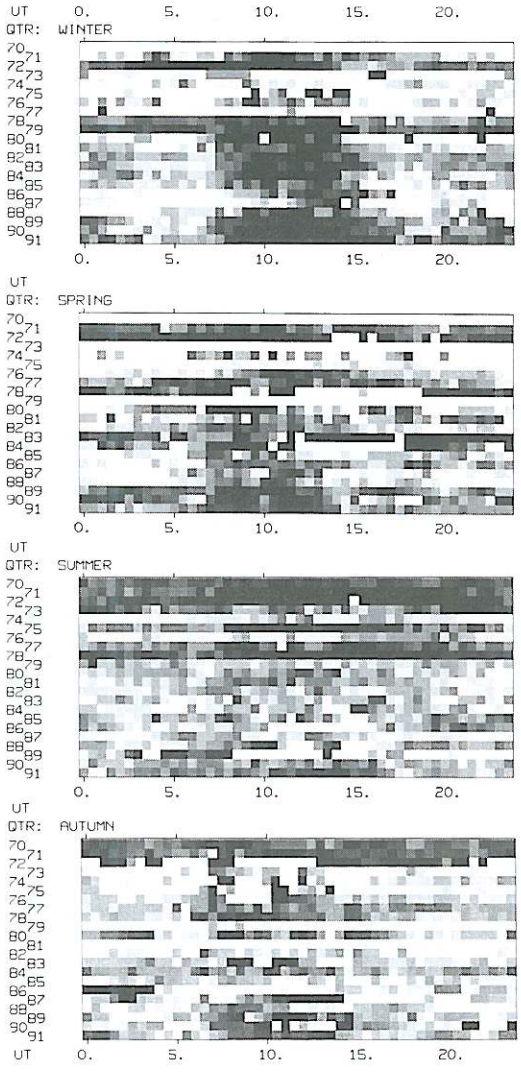

Fig. 17. Same as fig. 10a,b, but for a DM level of $2 \times 10^{11} \mathrm{m}^{-3}$. The grey level intervals are: 10-20, 20-30, 30-40, 40-50, 50-60, 60-70, 70-80 and > 80%.

Combining these data and those of section 5.1 we conclude that disturbances in the ionosphere are a common phenomenon. However, in Winter time the effect maximizes in daytime *i.e.*, around local noon. The pattern for the Spring, Summer and Autumn is much less pronounced while during several years any systematic pattern may even be absent.

This conclusion implies that in operational conditions the problem is not when the ionosphere is quiet or disturbed but which DM is acceptable for the application considered. Or: which DM gives an error in the results of the application within accepted tolerances.

It is not possible *a priori* to give a general answer to this question, also not in radio astronomy where the tolerance depends on *e.g.*, the observing technique and calibration method and possibilities. What certainly is possible is to query the present results more explicitely in view of the application considered and to determine an expectation of the effect on the results. To that end climatological data like those presented here should be included in dynamic ionospheric models.

8. Correction for ionospheric effects

Usually one is not satisfied with data affected by propagation effects. If possible one prefers to correct for these effects. In this section we describe correction procedures for ionospheric refraction and ionospheric Faraday rotation. A correction for ionospheric refraction should include estimates of both horizontal and vertical gradients in the electron density distribution. The accuracy of the available ionospheric data forms the basic limitation of the possible corrections.

Interferometric phase errors due to refraction can also be translated into errors in time delay, τ, and fringe rate, f (= $\nu \mathrm{d}\tau/\mathrm{d}t$). Also a procedure to correct VLBI observations for ionospheric refraction as suggested by Spoelstra (1984a,b) to indicate to which level this effect can be corrected by using total electron content, TEC, data. A discussion of the influence of the ionosphere on VLBI observational parameters and a correction procedure is reviewed in section 8.3.

8.1. *Faraday rotation*

Since the ionosphere is a magnetoionic medium the ionosphere is a doubly refractive

medium. It will support two orthogonal circularly polarized waves travelling with slightly different phase velocities. The ionosphere affects the state of polarization in the sense that the polarization ellipse is rotated. This is Faraday rotation, which also varies in inverse proportion to the observing frequency squared. Faraday rotation does not depolarize an arbitary ray – it is manifest in the interferometric amplitudes (section 4).

The correction for Faraday rotation is determined by eq. (4.9). In eq. (4.9) both the component of the geomagnetic field along the line of sight and the electron density integrated along the line of sight have to be known. For the geomagnetic field a model like the International Geomagnetic Reference Field may be used to sufficient accuracy. The slant total electron content can he determined from ionospheric soundings (section 9). By using eq. (4.9) the correction is straightforward.

8.2. *Ionospheric refraction: corrections for local interferometry*

8.2.1. Basic relations

The description of the influence of the ionosphere on the astrometric accuracy of radio astronomical observations may be simplified by the assumption that the process can be split into two independent parts:

1) refraction due to a spherically symmetric ionosphere;

2) (spatial and temporal variations of) refraction due to irregularities in the electron density distribution in the ionosphere.

In this discussion we use a spherical coordinate system, r, λ_g, β_g with origin at the centre of the Earth, where λ_g is the longitude measured eastward from the observer and β_g the geographical latitude. The determination of the electron density, N, as a function of the coordinates is in general restricted to an estimate of the columnar electron content (also called: column density), N_e. Note that N_e is also called the slant total electron content.

Refraction causes a shift of the position of extra-terrestrial objects on the celestial sphere: *i.e.*, of the celestial coordinates α (right ascension) and δ (declination). α is measured parallel to the celestial equator. δ is measured perpendicular to the celestial equator (the celestial North Pole is at $\delta = +90°$).

An expression for the total refraction due to a spherically symmetric ionosphere has been given by *e.g.*, Hagfors (1976). According to Chvojkova (1958a,b) and Komesaroff (1960) the apparent change of declination for a source at transit due to the spherical component of refraction, $\Delta\delta_s$, can be written as:

$$\Delta\delta_s = -\frac{df_0^2}{2r_m \nu^2} \sec^2 k_{0m} \tan k_{0m} \qquad (8.1)$$

where k_{0m} is the zenith angle at height r_m, the height of the maximum electron density.

The geometry is sketched in fig. 18, where several symbols are also defined. The apparent change of declination due to the horizontal electron density gradients, the «wedge component», $\Delta\delta_w$, is given by Komesaroff (1960) as

$$\Delta\delta_w = \frac{d\,\bar{\omega}(\sigma) \sec^2 k_{0m}}{2(r_b + \frac{3}{2} d)\nu^2} \frac{d(f_0^2)}{d\beta_g}. \qquad (8.2)$$

The parameter $\omega(\sigma)$ is given by

$$\omega(\sigma) = \frac{3}{4\sigma}\left[\frac{(1+\sigma)}{2\sqrt{\sigma}} \ln\left(\frac{(1+\sqrt{\sigma})}{(1-\sqrt{\sigma})}\right) - 1\right] \qquad (8.3)$$

where

$$\sigma = \frac{f_0^2}{\nu^2} \sec^2 k_{0m}. \qquad (8.4)$$

For values of σ lying between 0 and 0.5, $\bar{\omega}(\sigma)$ lies between 1 and 1.3. The change of right ascension depends (according to Komesaroff, 1960) to first order only on the east-west gradient in the electron density. He derives for this change the relation

$$\Delta\alpha = \frac{d\,\bar{\omega}(\sigma) \sec\delta \sec\phi_a \sec k_{0m}}{2(r_b + \frac{3}{2} d)\nu^2} \frac{d(f_0^2)}{d\lambda_g}. \qquad (8.5)$$

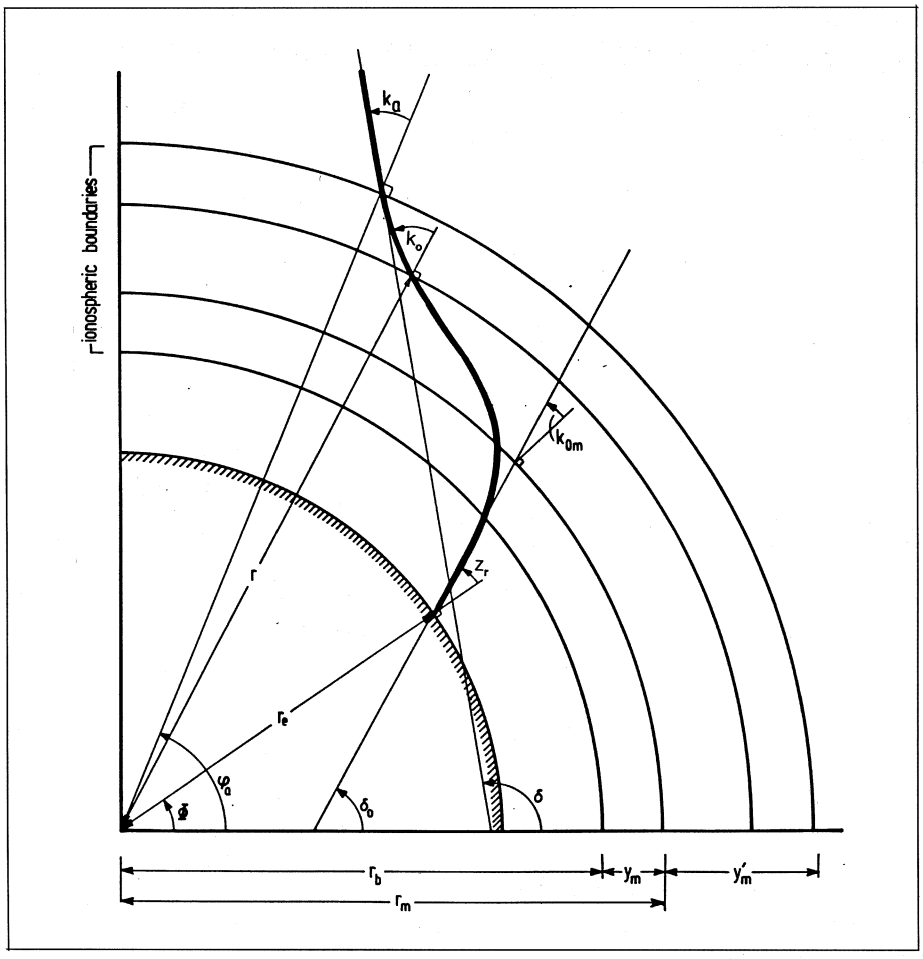

Fig. 18. Path of a ray through the ionosphere to an observer located at geographic latitude Φ. The equatorial plane is at Φ = 0°. (Not to scale) (based on Komesaroff, 1960).

To a sufficient accuracy ϕ_a can be written as

$$\sec\phi_a = \sec\beta_g \left[1 - \tan k_{0m} \tan\phi_0 \left(\frac{r_b - r_e + \frac{3}{2}d}{r_m}\right)\right]^{-1}. \tag{8.6}$$

The accuracy of $(\Delta\delta_s + \Delta\delta_w)$ is about 10% for sources up to about $k \approx 45°$ assuming that $\nu\sqrt{2}\,(f_0 F_2)$ sec k_{0m} which is certainly the case for WSRT observations.

As long as

$$\frac{\cos\delta}{\cos\beta_g}\cos k_{0m} \lesssim 1 \tag{8.7}$$

relation (8.6) has an accuracy of about 5%.

8.2.2. Discussion

An additional correction to get quantitatively the right corrections was found by taking

into account the vertical structure in the spherically symmetric component of the ionosphere (Spoelstra, 1983). Let the function $N(r)$ he obtained by distinguishing four zones within the F_2-layer (see fig. 19 for definitions). In this approximation we write for a zone:

$$f_0^2 = O + pr + 0.5\,qr^2 \tag{8.8}$$

were O, p and q are model parameters and r is the distance to the centre of the Earth. Then

$$\frac{d(f_0^2)}{dr} = p + qr. \tag{8.9}$$

In the present simple case the parameters p and q can be expressed per zone in a relation of the form

$$p = \frac{2sf_0^2 r}{(r_2 - r_1)(r_3 - r_1)} \tag{8.10}$$

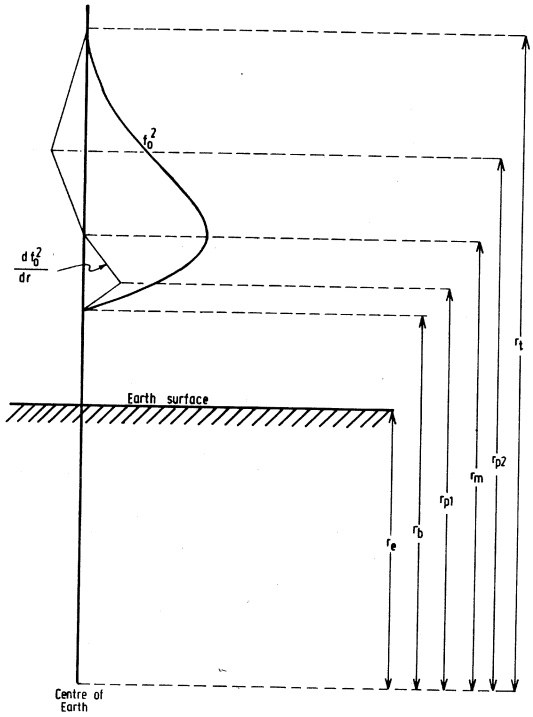

Fig. 19. Schematic presentation of vertical gradients in the electron distribution. The scales are arbitrary. Geometrical parameters are indicated.

Table IV. Indexed variables eq. (8.13).

Zone	p	q	s	r_1	r_2	r_3
1	p_1	q_1	-1	r_b	r_{p_1}	r_m
2	p_2	q_2	-1	r_m	r_{p_1}	r_b
3	p_3	q_3	$+1$	r_m	r_{p_2}	r_t
4	p_4	q_4	-1	r_t	r_{p_2}	r_m

and

$$q = \frac{-P}{r_1} \tag{8.11}$$

With the aid of table IV results can be obtained for the different zones. Then one can find that for zone i $\Delta\alpha$ due to refraction in the regular ionosphere is (De Munck, private communication)

$$\Delta\alpha = \frac{r_e \sin k_{0m}}{2v^2} A \tag{8.12}$$

with

$$A = \left[p_i \ln \left\{ \frac{r_k}{r_e \sin k_{0m}} + \left(\frac{r_k}{r_e^2 \sin^2 k_{0m}} - 1 \right)^{\frac{1}{2}} \right\} + q_i r_e \sin k_{0m} \left(\frac{r_k}{r_e^2 \sin^2 k_{0m}} - 1 \right)^{\frac{1}{2}} \right] +$$

$$+ \left[p_i \ln \left\{ \frac{r_j}{r_e \sin k_{0m}} + \left(\frac{r_j}{r_e^2 \sin^2 k_{0m}} - 1 \right)^{\frac{1}{2}} \right\} + q_i r_e \sin k_{0m} \left(\frac{r_j}{r_e^2 \sin^2 k_{0m}} - 1 \right)^{\frac{1}{2}} \right]. \tag{8.13}$$

Table V gives the appropriate values for the indexed variables in relations (8.12) and (8.13) for the four zones.

The correction procedure has been tested on WSRT observations (Spoelstra, 1983). Since the WSRT is aligned along an east-west line

Table V. Indexed variables eq. (8.13).

i	r_j	r_k
1	r_{p_1}	r_b
2	r_m	r_{p_1}
3	r_{p_2}	r_m
4	r_t	r_{p_2}

the «horizontal» errors are mainly due to the regular spherical component of the ionosphere and east-west gradients in the electron density. Ionospheric refraction may then be described by relation (8.5). Here the gradients appear in this relation as $d(f_0^2)/d\lambda_g$. The f_0F_2 information is usually available every hour and is thus not known continuously enough to calculate the gradients with the time resolution of the astronomical observation. Since gradients in λ_g are equivalent to gradients in time, relation (8.5) is approximated by assuming

$$\frac{d(f_0^2)}{d\lambda_g} = \frac{\Delta(f_0^2)}{\Delta t}, \qquad (8.14)$$

where

$$\frac{\Delta(f_0^2)}{\Delta t} = [0.5\{f_0F_2(t+1) + f_0F_2(t)\}]^2 + \\ -[0.5\{f_0F_2(t) + f_0F_2(t-1)\}]^2 \qquad (8.15)$$

and $f_0F_2(t)$ is the critical frequency of the F_2-layer at time t (t in integer hours). If only information from one ionosphere station can be used we are basically only able to account for horizontal east-west gradients in the electron density (or their equivalent as expressed by relation (8.14). This approximation is valid since the relatively large scale of horizontal variations in the electron density is several hundred kilometers. After correction deviations of the order of 1″ at decimeter wavelengths from the «true» astrometric position remain for the WSRT.

Komesaroff (1960) applied relations (8.1) through (8.7) to a number of discrete source observations taken with the Sydney 19.7 MHz Mills Cross with a beamwidth of 1.4°. His corrections for ionospheric refraction were mainly based on data from a number of ionospheric sounding stations close to the 150° meridian and 800-900 km apart. These formed the basis for the calculations of f_0 and north-south gradients. His results showed a very good improvement in declination. But after correction a systematic displacement in right ascension of about 3^m remained.

With this procedure to correct for ionospheric refraction it is possible to improve radio astronomical observations, except when ionospheric data show defects, irregularities at time scales less than the sampling time for the ionospheric parameters, and the correction needs to be determined for observations done during a few hours around sunrise (when the plasma is heated and vertical changes of this plasma occur).

8.3. *Ionospheric refraction: corrections for VLBI*

8.3.1. Basic equations

In general we cannot determine the values of the time delay, τ_D, and fringe rate, f, at any instant exactly when these are affected by refraction, due to several effects: *e.g.*, the rotation of the Earth; averaging over a finite integration time, and sampling the data at discrete time intervals rather than continuously; unknown offsets in time and frequency; effects due to the Earth's atmosphere (*e.g.*, Cohen and Shaffer, 1971).

The observed time delay τ_0 between two elements of the interferometer is given by

$$\tau_0 = \frac{B}{c}\sin d \sin\delta + \\ + \frac{B}{c}\cos d\cos\delta\cos(\alpha - h) + \Delta\tau_c + \Delta\tau_a \qquad (8.16)$$

where (d, h) is the orientation of the baseline, $\Delta\tau_c$ denotes the influence of clock errors, of the rotation of the Earth, etc., and atmospheric errors (*i.e.*, due to troposphere and ionosphere)

are included in $\Delta\tau_a$. Equation (8.16) can also he written as

$$\tau_0 = \frac{l_1}{c}\sin\delta + \frac{l_2}{c}\cos\delta\cos(\alpha - h) + \Delta\tau_c + \Delta\tau_a \tag{8.17}$$

where $l_1 = B \sin d$ and $l_2 = B \cos d$. The rotation of the Earth causes h to vary with time. The rate of change of the delay τ_D is given by

$$\frac{d\tau_D}{dt} = -\frac{l_2}{c}\cos\delta\sin(\alpha - h)\frac{dh}{dt}. \tag{8.18}$$

Then the fringe rate f due to the Earth's rotation is

$$f = \nu\frac{d\tau_D}{dt} = -\frac{dh}{dt}\frac{\nu}{c}l_2\cos\delta\sin(\alpha - h) = $$

$$= -\Omega l'_2\cos\delta\sin(\alpha - h) \tag{8.19}$$

where Ω is the angular velocity due to the Earth's rotation. Then the observed fringe frequency can be written as

$$f_{\text{obs}} = -\Omega l'_2\cos\delta\sin(\alpha - h) + \Delta f_c + \Delta f_a \tag{8.20}$$

where Δf_c denote the influences of clock errors, of the rotation of the Earth, etc., while atmospheric errors are included in Δf_a.

If we neglect the influence of the troposphere relations (8.17) and (8.20) describe the influence of the ionosphere if we neglect the influences of clock errors, of the rotation of the Earth, etc. (*i.e.*, $\Delta\tau_c = \Delta f_c = 0$). The terms $\Delta\tau_a$ and Δf_a can be expressed in terms of the changes in α and δ due to (ionospheric) refraction. $\Delta\alpha$ and $\Delta\delta$ respectively. If the true values of α and δ are written as α_0, δ_0 we can rewrite eq. (8.17) as

$$\tau_D = \frac{l_1}{c}(\sin\delta_0 + \Delta\delta\cos\delta_0) +$$

$$+\frac{l_2}{c}\{\cos\delta_0\cos(\alpha_0 - h) - \Delta\alpha\cos\delta_0\sin(\alpha_0 - h) +$$

$$-\Delta\delta\sin\delta_0\cos(\alpha_0 - h)\} \tag{8.21}$$

and relation (8.20) as

$$f_{\text{obs}} = -\Omega l'_2\{\cos\delta_0\sin(\alpha_0 - h) +$$

$$+\Delta\alpha\cos\delta_0\cos(\alpha_0 - h) - \Delta\delta\sin\delta_0\sin(\alpha_0 - h). \tag{8.22}$$

The terms $\Delta\tau_a$ and Δf_a in relations (8.16) and (8.17) can now he written as

$$\Delta\tau_a = \frac{l_1}{c}\Delta\delta\cos\delta_0 +$$

$$-\frac{l_2}{c}\{\Delta\alpha\cos\delta_0\sin(\alpha_0 - h) + \Delta\delta\sin\delta_0\cos(\alpha_0 - h)\} \tag{8.23}$$

and

$$\Delta f_a = -\Omega l'_2\{-\Delta\alpha\cos\delta_0\cos(\alpha_0 - h) +$$

$$+\Delta\delta\sin\delta_0\sin(\alpha_0 - h)\} \tag{8.24}$$

where α_0 and δ_0 give the true source position.

The basic relations for the determination of $\Delta\alpha$ and $\Delta\delta$ due to ionospheric refraction were given by *e.g.*, Spoelstra (1983). Relations (8.23) and (8.24) can be used as a description of the influence of ionospheric refraction on observational parameters of all interferometer systems including VLBI.

In VLBI an important problem is that the line of sight for each element of the interferometer points through a part of the atmosphere whose physical state is uncorrelated with that of all other elements. If we assume that to first order the refraction is the arithmetic mean of the contributions by the atmosphere above each of the n interferometer elements, $\Delta\alpha$ and $\Delta\delta$ can be written as

$$\Delta\alpha = \frac{1}{n}\sum_{i=1}^{n}\Delta\alpha_i \quad \text{and} \quad \Delta\delta = \frac{1}{n}\sum_{i=1}^{n}\Delta\delta_i. \tag{8.25}$$

Here $\Delta\alpha$ and $\Delta\delta$ indicate the magnitude of the total refraction error; the corrections are applied to each interferometer independently.

For each element $\Delta\alpha$ can be derived using the method described in section 8.2. The

F_2-layer of the ionosphere dominates ionospheric influences at the frequencies used. The columnar electron density, N, of the F_2-layer can be derived from observations of the critical frequency, f_0F_2 of the F_2-layer. The f_0F_2 values can be derived from ionosonde observations. Since east-west gradients giving rise to $\Delta\alpha$ are equivalent to gradients in time, continuous time series of f_0F_2 observed at an ionosonde station close to an element of the interferometer (*e.g.*, at a distance less than 100-200 km) are needed to calculate $\Delta\alpha$ for the line of sight of that element (Spoelstra, 1983).

The determination of $\Delta\delta$ cannot be made with the simple assumptions used for the calculation of $\Delta\alpha$. Komesaroff (1960) determined the north-south gradients giving rise to $\Delta\delta$ from observations by a network of ionosonde stations. More accurate information on gradients in the ionospheric electron density distribution is of course provided by satellite data.

When $\Delta\alpha$ and $\Delta\delta$ are determined in this way, the corrections given by relations (4.6) and (4.7) can be calculated.

8.3.2. Application and discussion

Ionospheric refraction affects the astrometric accuracy of radio astronomical observations. The errors can easily be in the order of several seconds of arc. These position shifts may influence identification with sources at higher (*i.e.*, optical) frequencies, while features in extended objects may change in position and structure due to ionospheric refraction. Variations of ionospheric refraction on a time scale less than the one at which the corrections are applied may show up as spokes around point sources (*e.g.*, Hinder and Ryle, 1971). It is possible to clean the maps for these disturbances by other techniques, *e.g.*, by using model fitting or closure phase techniques (*e.g.*, Noordam and De Bruyn, 1982). These procedures may result in fine images of the observed field, but cannot improve astrometric accuracy.

Spoelstra (1995) showed that with the aid of the method described here, the time delay errors, $\Delta\tau_a$, and fringe rate errors, Δf_a, can be calculated with an accuracy of a few centimetres for 1000 km baselines if a network of both ionosonde and satellite tracking stations «co-located» with the VLBI stations, is operational during the astronomical observations. On the basis of the information provided by these ionosphere stations the VLBI observations can be corrected adequately. This will improve the absolute astrometric accuracy of the results.

Using the approach by Spoelstra (1983) as summarized in section 8.2.1 we are able to correct for these errors with an accuracy of typically 15%. This accuracy is also reached when values for N are used which have been determined from differential Doppler observations of navigation satellites. The accuracy of N is typically 10% (Leitinger *et al.*, 1975; Leitinger and Putz, 1978).

The dual frequency technique has the advantage that for the calibration, correction and reduction of the data no additional information about the ionosphere is necessary. But in case celestial sources are observed an error may occur if the spectral index of the observed radio waves varies over the source. This method is, however, not commonly used in VLBI campaigns since only a limited number of VLBI stations is equipped with this facility.

9. Determination of ionospheric electron content

The most important parameters for corrections for ionospheric effects are the electron content integrated along the line of sight and gradients in the electron density distribution perpendicular and along the line of sight. This slant total electron content, or slant TEC, and the gradients mentioned cannot be measured directly. However, by means of vertical and oblique sounding techniques measurements can be made of the critical frequency of the different ionospheric layers and other ionospheric parameters. This is especially true for the critical frequency of the F_2 layer, f_0F_2, which is relevant for radio astronomy interferometry. Other techniques which inform us on the ionospheric electron density distribution are satellite-bound, like Faraday rotation of the polarization angle of the signal transmitted by the

satellite, differential Doppler measurements using dual frequency satellite beacon signals and range measurements by means of satellite signals. These data also contain information on the ionospheric electron density distribution.

In this context it is important to know that the instrumental beamwidth used by vertical and oblique sounders is several tens of degrees (typically 40°-60°), which implies that only the very large scale electron distribution can be monitored. Usually these sounding measurements are done hourly, which is usually sufficient given the beam of the instruments used. Satellites have small angular dimensions in the sky, so satellite measurements are basically measurements of discrete point sources. This implies that satellite measurements can provide significant information on the small scale spatial and temporal variations in the ionospheric electron distribution.

Vertical and oblique sounding techniques inform us mainly about one side of the ionosphere: the bottomside for Earth-based experiments and the topside of space-borne experiments. Since the satellites commonly used for probing the ionosphere fly above about 1000 km there orbits are largely outside the ionosphere. Therefore, they should give information about the ionosphere electron content integrated along the whole line of sight from the observer towards the satellite.

9.1. *Limitations of vertical/oblique sounding measurements*

Vertical and oblique sounding techniques have the following important limitations:

1) they provide mainly information on one side of the ionosphere as mentioned above as *e.g.*, f_0F_2, values;

2) since the *distribution* of the ionospheric electrons along and perpendicular to the line of sight is not known the measured parameter can only be converted into TEC information if a model of the ionosphere is used. Often as a model one assumes that the vertical distribution of ionospheric electron with height corresponds to a parabola having a width equivalent to the equivalent thickness of the ionosphere. The accuracy of the determination of the slant TEC is then usually not better than about 15%;

3) given the large antenna beamwidths the method is not suitable to determine small scale electron density variations.

Satellite measurements might alleviate these limitations. In principal they should provide better ionospheric information especially when they move well above the ionosphere.

9.2. *Differential Doppler technique*

Differential Doppler measurements can be performed using the satellites of *e.g.*, the Navy Navigation Satellite System, NNSS. The NNSS satellite system consists of five satellites moving in polar orbits at 1100 km altitude. They are transmitting coherently two signals at frequency of 150 and 400 MHz. The phase path of these signals is decreased due to the presence of the ionosphere.

The phase path ϕ_N can he expressed as

$$\phi_N = \frac{1}{\lambda} + \nu t = \frac{\nu L}{c} + \nu t \quad \text{(Hz)}, \qquad (9.1)$$

where the optical path $L = \int_s n\,ds$, ν is the frequency, t is time, λ is the wavelength, c the speed of light and n is the real part of the refractive index. The decrease of the phase path due to the refractive medium, $\Delta\phi_N$, equals can he expressed in units of the Total Electron Content, TEC, as

$$\Delta\phi_N = \frac{1.34\times10^{-7}}{\nu}\,\text{TEC} \qquad (9.2)$$

(Kelder and Spoelstra. 1984). The quantity TEC can he expressed as

$$\text{TEC} = \frac{1}{\cos k_0}\int_s N(r)ds = DN_p, \qquad (9.3)$$

where D is a geometrical factor (Leitinger and Putz, 1978; Kelder and Spoelstra, 1984). A frequency shift, $\Delta\nu$, being the consequence of the time dependent phase shift can be written as

$$\Delta\nu = \frac{d\Delta\phi_N}{dt} = \frac{1.34\times10^{-7}}{\nu}\frac{d}{dt}(\text{TEC}). \qquad (9.4)$$

Thus the frequency shift is a direct manifestation of the variations in TEC (Leitinger and Putz, 1978; Kelder and Spoelstra, 1984).

Every time the receiver locks to the signal, the differential phase count starts at some number. In other words, for every satellite pass there is at least one unknown offset in $\Delta\phi$. An unknown offset in $\Delta\phi$ results in an unknown offset in TEC. In systems where (Doppler) frequency shift rather than phase difference is measured, the unknown constant corresponds to a constant of integration (frequency being the derivative of phase). Considerable research has been invested in methods to determine this unknown offset (*e.g.*, Leitinger and Putz, 1978). All these methods assume implicitely that the ionosphere is an infinitesimally thin layer at ionospheric height. The so-called one station methods, with only one ground-based receiver, further assume smooth variations (usually linear) of the electron content distribution. The latter two assumptions are basically some kind of *a priori* ionospheric *model* put into the determination of TEC and its variations.

9.3. *Range measurements*

Other than by using differential Doppler measurements of satellites of the Navy Navigation Satellite System, NNSS, TEC observations can be made by range measurements of satellites of the U.S. Global Positioning System, GPS, and the Russian GLONASS system (*e.g.*, Spoelstra, 1987a,b).

Both systems operate at a couple of *L*-band frequencies. The center-frequencies for the different GPS frequency bands are: *L*1 = 1575.42 MHz, *L*2 = 1227.60 MHz and *L*3 centered at 1381.05 MHz. GLONASS operates at various frequencies for *L*1 and *L*2 bands. In fact, the frequencies at which the GLONASS satellites operates can be changed within a range of about 15 MHz. This is not the case for GPS satellites. A second difference between GPS and GLONASS is that each GPS satellite has its own clock, while all GLONASS satellites use the same clock.

Both systems encrypt the transmitted signal with a course and a precise code, respectively annotated by *C/A* and *P*.

For the present discussion we evaluate GPS measurements to determine TEC.

On January 31st, 1994, 0 h 00 min UT, Anti-Spoofing (A-S), was turned on for most GPS satellites (of the so-called block II satellites). When *A-S* is on, the *P*-code is replaced by a secret *Y*-code (currently the *P*-code is encryptic) to protect military receivers against jamming. Only military receivers with the appropriate key can use the *Y*-code directly. Other dual-frequency GPS receivers have to rely on:

a) *signal-squaring on L2* (Trimble SST, Leica, and many others); this gives *C/A*-code and phase observations on *L*1, and phase observations on *L*2 with half wavelength (no *L*2 code);

b) *cross-correlation* (Trimble 4000 SSE, Turbo Rogue); this gives *C/A*-code and phase observations on *L*1, and differential code (*Y*2-*Y*1) and phase (*L*2-*L*1) observations, from which code and phase observations on *L*2 can be constructed;

c) *P/W tracking* (Ashtech Z12); this gives a sort of *P*-code and phase observations on both *L*1 and *L*2.

Although cross-correlation and *P/W* tracking give code and (full-wavelength) phase measurements on *L*2, they have their disadvantages: they must use the *C/A* code instead of the more precise *P*-code (cross-correlation, signal-squaring) and the signal-to-noise ratio is lower than when *P*-code observations are used directly. *P/W* tracking is claimed to give the best results in terms of signal-to-noise ratio, followed by cross-correlation. Therefore, when *A-S* is on, the precision of the measurements will be degraded.

There is another deliberate effect which is introduced for US security reasons: this is the so-called Selective Availability (SA). Fortunately, TEC determinations are not affected by SA, because the effect is the same for both frequencies.

9.3.1. TEC-estimates from dual-frequency GPS

It is highly desirable to be able to make measurements of TEC to an absolute accuracy of 1 TEC unit (= 10^{16} el/m^{-3}), since nightime

absolute TEC values can be as low as 1 TEC unit during solar minimum. One nanosecond of GPS differential code delay corresponds to 2.852 TEC units. Thus during solar minimum time of low electron content, the total differential code delay from the ionosphere can be approximately 1/3 of a nanosecond, and an accuracy in the determination of group delay values to this order is highly desirable.

Several workers have made estimates of the group delay values from various GPS satellites. In these estimates the use of an ionospheric «shell-like» model with a fixed height of typically about 350 km is quite common (*e.g.*, Lanyi, 1986; Coco *et al.*, 1991; Gaposchkin and Coster, 1993; Sardon and Wanniger, 1993; Wanniger and Sardon, 1993). A significant problem is the determination of biases for the transmitter and receiver systems and for the slant ionospheric delay. Various methods have been proposed to solve or reduce this problem ranging from a Kalman filter approach to the development of a many order polynomial function (Wanniger *et al.*, 1994 and Van der Marel and Georgiadou, 1994, respectively).

In addition, all the methods of determining the TEC used by workers to date implicitely neglected the effects of the electrons in the Earth's protonosphere. They have all, in some form or other, used an ionospheric «shell» model, which does not include the contribution to electron content of the Earth's protonosphere in different viewing directions during a typical GPS satellite pass. It is, however, well known that the relative effects of the electron content of the Earth's protonosphere can be up to 50% of the entire TEC during the nightime, and 10% of the TEC during the day (Davies, 1980). Since a typical GPS satellite observed from a given station covers a widely different portion of the protonosphere over the course of its pass, it can be expected that any simple «shell» model of the ionosphere will not be an accurate representation of the actual behaviour of TEC over the pass.

Klobuchar *et al.* (1994) estimated that the accuracy of TEC from GPS measurements based on group delay measurements is likely to be not better than ~ 5 TEC units (1-2 nanoseconds group delay accuracy) at the present time. This is due to neglecting the contribution of the Earth's protonosphere to the TEC. Potential improvements can be made by using a model of the protonosphere to subtract this contribution before the present ground-based methods of using a «shell-like» ionosphere are assumed. Another potential method of directly measuring the group delay is to monitor signals from GPS satellites from a latitude poleward of the plasmapause at a time when the ionospheric contribution is small.

In addition the biases mentioned cause uncertainties, although attempts to model the satellite and receiver biases seem promising (Van der Marel and Georgiadou, 1994). The accuracy of the determination of TEC variations is probably an order of magnitude better than of absolute TEC as various investigators show. Given the uncertainties in the «model-assumptions» for the TEC determination by means of GPS, the physical meaning of the derived results deserves attention.

On the basis of a preliminary comparison between TEC information derived from a chirpsounder, an ionosonde and GPS data, Van der Marel and Spoelstra (1994) confirmed the accuracy estimate of Klobuchar *et al.* (1994) the TEC determination by means of GPS. For radio astronomy this implies that the use of GPS to correct for ionospheric influences on the observations does not yet give accuracies sufficiently good to produce results of adequate astronomical accuracy. In fact, the achievable accuracy of TEC determinations restrict the achievable accuracy of the corrections for ionospheric effects on radio astronomical results is similar to that of other techniques, like ionosonde. In practice this TEC information is about $(3/\nu)$ times less accurate than the desired tolerance for radio astronomical maps with a dynamic range of 30 dB is (here ν is in GHz).

It should he noted that these accuracies refer to *absolute* TEC data. *Relative* TEC data which show the variations of TEC with coordinate and time may have a better accuracy. For radio astronomy both absolute and relative TEC values are relevant: absolute values for ionospheric Faraday corrections and both absolute and relative for ionospheric refraction corrections.

10. Conclusions

In this review we addressed the question of the influence of the ionosphere on radio astronomical observations. This question has been be approached from the interest of aeronomy and as a problem which affects the quality of radio astronomical measurement results: *i.e.*, the ionosphere as an object of study and the ionosphere as a nuisance.

Radio interferometry has proven to provide a powerful tool to sense the refractive medium, in particular to investigate various characteristics of the irregularities in this medium – such as their spatial and temporal behaviour, climatology, location within the ionosphere, and their effect on the radio astronomical observations. This holds particularly for phenomena related to TIDs and scintillation. A radio interferometer as one single instrument enables a kind of «multi-dimensional» study of the ionospheric problems space.

In general, the sensitivity for ionospheric effects in different aspects of radio communication and signal detection depends on the kind of application selected and the analysis of the data. In radio interferometry, the large scale characteristics cannot be studied very well, since interferometry is primarily sensitive for differential effects along the line of sight from the telescope pairs.

Acknowledgements

The Westerbork Synthesis Radio Telescope is operated by the Netherlands Foundation for Research in Astronomy with financial support from the Netherlands Organization for the Advancement of Research (NWO).

REFERENCES

ALCAYDE, D. (1974): Diurnal and long-term behaviour of the exospheric temperature as observed by incoherent scatter sounding in the F_2-region, *Radio Sci.*, **9**, 239-245.

BAARS, J.W.M., J.F. VAN DER BRUGGE, J.L. CASSE, J.P. HAMAKER, L.H. SONDAAR, J.J. VISSER and K.J. WELLINGTON (1973): The synthesis radio telescope at Westerbork, *Proceedings IEEE*, **61**, 1258-1266.

BELYAEV, N.A. (1955): *Astron. J. Moscow*, **32**, 357.

BOOKER, H.G. (1979): The role of acoustic gravity waves in the generation of spread-*F* and ionospheric scintillation, *J. Atmos. Terr. Phys.*, **41**, 501-515.

BOS, A., E. RAIMOND and H.W. VAN SOMEREN GRÉVE (1981): A digital spectrometer for the Westerbork synthesis radio telescope, *Astron. Astrophys.*, **98**, 251-259.

BROUW, W.N. (1969): Netherlands Foundation for Radio Astronomy, *Internal Technical Report*, No. 78.

BROUW, W.N. (1971): Data processing for the Westerbork Synthesis Radio Telescope, *Ph.D. Thesis*, Leiden University.

CANZIANI, P.O. (1994): On tidal variability and the existence of planetary wave-like oscillations in the upper thermosphere – I. Observations of tidal variability, *J. Atmos. Terr. Phys.*, **56**, 901-912.

CASSE, J.L. and C.A. MULLER (1974): The synthesis radio telescope at Westerbork. The 21 cm continuum receiver system, *Astron. Astrophys.*, **31**, 333-338.

CHAPMAN, S. and R.S. LINDZEN (1970): *Atmospheric Tides* (Reidel, Dordrecht).

CHVOJKOVA, E. (1958a): Refraction of radio waves in an ionized medium-I: waves from radio stars crossing spherical layers, *Bull. Astron. Inst. Csl.*, **9**, 1-9.

CHVOJKOVA, E. (1958b): Refraction of radio waves in an ionized medium-III: arbitrary electron distribution, *Bull. Astron. Inst. Csl.*, **9**, 133-138.

COCO, D.S., C.E. COKER, S.R. DAHLIE and J.R. CLYNCH (1991): *IEEE Trans. Aerosp. Electron. Syst.*, **27** (6), 931.

COHEN, M.H. and D.B. SHAFFER (1971): Positions of radio sources from long-baseline interferometry, *Astron. J.*, **76**, 91-100.

DAVIES, K. (1980): *Space Science Reviews*, **25**, 357.

DRAZIN, P.G. and W.H. REID (1981): *Hydrodynamic Stability* (Cambridge University Press).

DYSON, P.L., J.P. MCCLURE and W.B. HANSON (1974): *In situ* measurements of amplitude and scale size characteristics of ionospheric irregularities, *J. Geophys. Res.*, **79**, 1479.

EVANS, J.V. (1983): A differential Doppler study of traveling ionospheric disturbances from Millstone Hill, *Radio Sci.*, **18**, 435-451.

FOMALONT, E.B. (1973): Earth-rotation aperture synthesis, *Proceedings IEEE*, **61**, 1211-1218.

FRITTS, D.C. and R.A. VINCENT (1987): *J. Atmos. Sci.*, **44**, 605-619.

GAPOSCHKIN, E.M. and A.J. COSTER (1993): Lincoln Laboratory, *Technical Report*, No. 971, 12 January 1993.

GAVRILOV, N.M., B.V. KAL'CHENKO, B.L. KASHCHEYEV and G.M. SHVED (1981): Discovery of a relationship between the intensity of internal gravity waves in the upper atmosphere and the tidal phase, *Izv., Atmos. Oceanic Phys.*, **17**, 499-505.

HAGFORS, T. (1976): The ionosphere, in *Astrophysics*, edited by M.L. MEEKS (Academic Press, London), vol. 12B, p. 119.

HAMAKER, J.P. (1978): Atmospheric delay fluctuations with scale sizes greater than one kilometer, observed with a radio interferometer array, *Radio Sci.* **13**, 873-981.

HINDER, R. and M. RYLE (1971): Atmospheric limitations to the angular resolution of aperture synthesis radio telescope, *Mont Not. R. Astron. Soc.*, **154**, 229-253.

HÖGBOM, J.A. and W.N. BROUW (1974): The synthesis radio telescope at Westerbork. Principles of operation, performance and data reduction, *Astron. Astrophys.*, **33**, 289-301.

KALIKHMAN, A.D. (1980): Medium-scale travelling ionospheric disturbances and thermospheric winds in the *F*-region, *J. Atmos. Terr. Phys.*, **42**, 697-703.

KELDER, H. and T.A.TH. SPOELSTRA (1984): Multi-technique study of medium scale TIDs, *Kleinheubacher Berichte*, No. 27, 575-584.

KELDER, H. and T.A.TH. SPOELSTRA (1987): Medium scale TIDs observed by radio interferometery and differential Doppler techniques, *J. Atmos. Terr. Phys.*, **49**, 7-17.

KLOBUCHAR, J.A., P.H., DOHERTY, G.J. BAILEY and K. DAVIES (1994): Limitations in determining absolute total electron content from dual-frequency GPS group delay measurements, in *Proceedings of the International Beacon Satellite Symposium, 11-15 July 1994*, edited by L. KERSLEY, University of Wales, Aberystwyth, p. 1.

KOMESAROFF, M.M. (1960): Ionospheric refraction in radio astronomy, *Aust. J. Phys.*, **13**, 153-167.

KUMAGAI, H. (1987): Spatial correlations in intense ionospheric scintillations: comparison between numerical computation and observation, *Radio Sci.*, **22**, 439-448.

LANYI, G. (1986): in *Proceedings of the International Beacon Satellite Symposium, part II*, edited by A. TAURIAINEN, Oulu University, June 1986.

LEITINGER, R. and E. PUTZ (1978): Pie Auswertung von Differenz-Doppler-Messungen an den Signalen von Navigationssatelliten, Technischer Bericht, Institut für Meteorologie und Geophysik der Universität Graz.

LEITINGER, R., G. SCHMIDT and A. TAURIAINEN (1975): An evaluation method combining the differential Doppler measurements from two stations that enables the calculation of the electron content of the ionosphere, *J. Geophys.*, **41**, 201-213.

LINK, F. (1957): *Bull. Astron. Inst. Csl.*, **8**, 112.

MERCIER, C. (1986): Observations of atmospheric gravity waves by radio interferometry, *J. Atmos. Terr. Phys.*, **48**, 605-624.

MERCIER, C. (1996): Some characteristics of atmospheric gravity waves observed by radio-interferometry, *Ann. Geophys.*, **14**, 42-58.

MERCIER, C., F. GENOVA and M.G. AUBIER (1989): Radio observations of atmospheric gravity waves, *Ann. Geophys.*, **7**, 195-202.

MUNRO, G.H. (1958): Travelling disturbances in the ionosphere, *Proc. R. Soc. Ser. A.*, **202**, 208-223.

NOORDAM, J.E. and A.G. DE BRUYN (1982): High dynamic range mapping of radio sources, with application to 3C84, *Nature*, **299**, 597-600.

RUFENACH, C.L. (1972): Power law wave number spectrum deduced from ionospheric scintillation observation, *J. Geophys. Res.*, **77**, 4761-4772.

SAGALYN, R.C., M. SMIDDY and J. WISNIA (1973): Measurement and interpretation of ion density distribution in the daytime, *J. Geophys. Res.*, **69**, 199.

SARDON, E. and L. WANNINGER (1993): IfE-MEMO WA-03/93, Hannover University, March 1993.

SPOELSTRA, T.A.TH. (1983): The influence of ionospheric refraction on radio astronomy interferometry, *Astron. Astrophys.*, **120**, 313-321.

SPOELSTRA, T.A.TH. (1984a): Correcting radio astronomy interferometry for ionospheric refraction, in *«Characteristics of the Lower Atmosphere Influencing Radio Wave Propagation», AGARP Conference Proceedings*, No. 346, 15-18.

SPOELSTRA, T.A.TH. (1984b): Correcting VLBI-observations for ionospheric refraction, in *Proceedings of the International Symposium on «Beacon Satellite Studies of the Earth's Environment», February 7-11, 1983* and *Workshop on «Beacon Techniques and Applications», February 3-4, 1983*, edited by T.R. TYAGI, New Delhi, p. 439.

SPOELSTRA, T.A.TH. (1985): Effects of amplitude and phase scintillation on decimeter wavelength observations at mid-latitudes, *Astron. Astrophys.*, **148**, 21-28.

SPOELSTRA, T.A.TH. (1987a): Correcting refraction in radio astronomy, *Publ. Astr. Ops. Beograd*, No. 35, 213-241.

SPOELSTRA, T.A.TH. (1987b): Correcting refraction in radio astronomy and satellite geodesy, *Kleinheubacher Berichte*, **30**, 1-13.

SPOELSTRA, T.A.TH. (1992a): Ionosphere and troposphere seen through a radio interferometer, in *«Remote Sensing of the Propagation Environment», AGARP Conference Proceedings*, No. 502, 16-1-10.

SPOELSTRA, T.A.TH. (1992b): Combining TID observations: NNSS and radio interferometry data, *J. Atmos. Terr. Phys.*, **54**, 1185-1195.

SPOELSTRA, T.A.TH. (1995): Correcting VLBI observations for ionospheric refraction, *J. Atmos. Terr. Phys.*, **57**, 163-167.

SPOELSTRA, T.A.TH. (1996): A climatology of quiet/disturbed ionospheric conditions derived from 22 years of Westerbork interferometer observations, *J. Atmos. Terr. Phys.*, **58**, 1229-1258.

SPOELSTRA, T.A.TH. and H. KELDER (1984): Effects produced by the ionosphere on radio interferometry, *Radio Sci.*, **19**, 779-788.

SPOELSTRA, T.A.TH. and YANG YI-PEI (1995): Ionospheric scintillation observations with radio interferometry, *J. Atmos. Terr. Phys.*, **57**, 85-98.

THOMPSON, A.R. (1989): The interferometer in practice, in *Synthesis Imaging in Radio Astronomy*, edited by R.A. PERLEY, F.R. SCHWAB and A.H. BRIDLE, *Astronomical Society of the Pacific Conference Series*, vol. 6, p. 11.

TITHERIDGE, J.E. (1968): Periodic disturbances in the ionosphere, *J. Geophys. Res.*, **73**, 243-252.

VAN DER MAREL, H. and Y. GEORGIADOU (1994): TEC-observations from GPS under Anti-Spoofing, in *Proceedings of the International Beacon Satellite Symposium, 11-15 July 1994*, edited by L. KERSLEY, University of Wales, Aberystwyth, p. 5.

VAN DER MAREL, H. and T.A.TH. SPOELSTRA (1994): Comparison of ionospheric Corrections from GPS, Chirpsounder and Ionosonde data for radio astronomy, in *Proceedings of the International Beacon Satellite Symposium, 11-15 July 1994*, edited by L. KERSLEY, University of Wales, Aberystwyth, p. 354.

VAN SOMEREN GRÉVE, H.W. (1974): The data handling of the Westerbork synthesis radio telescope, *Astron. Astrophys. Suppl. Series*, **15**, 343-352.

VAN VELTHOVEN, P.F.J. (1990): Medium scale irregularities in the ionospheric electron content, *Ph.D. Thesis*, Eindhoven University of Technology.

VAN VELTHOVEN, P.F.J., C. MERCIER and H. KELDER (1990): Simultaneous observations of travelling ionospheric disturbances by two-dimensional radio interferometry and the differential Doppler technique applied to satellite signals, *J. Atmos. Terr. Phys.*, **52**, 305-312.

WALDOCK, J.A. and T.B. JONES (1986): HF Doppler observations of medium-scale travelling ionospheric disturbances at mid-latitudes, *J. Atmos. Terr. Phys.*, **48**, 245-260.

WANG HONG, XINMIN WANG, SHOUGUAN WANG, FUYOU LIU, TINGYI PU, HONGSHEN CHEN, YUHAI QIU, YIPEI YANG, LEI PANG, CHUNLU ZHANG, GUOQUAN ZHANG, XIZHEN ZHANG, TIELIN JIN, YIJIA ZHEN, HUIPING ZHAO, RENDONG NAN, LIANSHENG KANG, HONGQI BAO and MINGZHI WEI (1986): Mi Yun synthesis radio telescope, *Chin. Astron. Astrophys.*, **10**, p. 3 (1985, *Act. Astrophys. Sin.*, **5**, p. 245).

WANNINGER, L. and E. SARDON (1993): IfE-MEMO WA-09/93, Hannover University, September 1993.

WANNINGER, L., E. SARDON and E. WARNANT (1994): Determination of the total ionospheric electron content with GPS – difficulties and their solution, in *Proceedings of the International Beacon Satellite Symposium, 11-15 July 1994*, edited by L. KERSLEY, University of Wales, Aberystwyth, p. 5.

WEENINK, M.P.H. (1987): A new method for the calculation of the phase path in the geometrical-optics approximation, *Manuscripta Geodaetica*, **12**, 99-103.

WERNIK, A.W. and C.H. LIU (1975): Application of the scintillation theory to ionospheric irregularity studies, *Artificial Satellites*, **10**, 37-58.

YEH, K.C. and C.H. LIU (1980): Statistical properties of transionospherically propagated radio signals under intense scintillation conditions, in *AGARD Conference Proceedings*, No. 284, *Propagation Effects in Space/ Earth Paths*, 30-31.

YEH, K.C. and C.H. LIU (1982): Radio wave scintillations in the ionosphere, in *Proceedings IEEE*, **70**, 324-360.

(received September 24, 1996;
accepted May 7, 1997)